DISCLAIMER

This report was prepared as an account of work sponsored by an agency of the United States Government. Neither the United States Government nor any agency thereof, nor any of their employees, makes any warranty, express or implied, or assumes any legal liability or responsibility for the accuracy, completeness, or usefulness of any information, apparatus, product, or process disclosed, or represents that its use would not infringe privately owned rights. Reference herein to any specific commercial product, process, or service by trade name, trademark, manufacturer, or otherwise does not necessarily constitute or imply its endorsement, recommendation, or favoring by the United States Government or any agency thereof. The views and opinions of authors expressed herein do not necessarily state or reflect those of the United States Government or any agency thereof. Reference herein to any social initiative (including but not limited to Diversity, Equity, and Inclusion (DEI); Community Benefits Plans (CBP); Justice 40; etc.) is made by the Author independent of any current requirement by the United States Government and does not constitute or imply endorsement, recommendation, or support by the United States Government or any agency thereof.

Argonne NATIONAL LABORATORY

ANL/RTR/TM-23/13

Irradiation Thermo-Mechanical Modeling and Analysis of University of Missouri Research Reactor HEU Fuel Plates

Nuclear Science & Engineering Division

ANL/RTR/TM-23/13

Irradiation Thermo-Mechanical Modeling and Analysis of University of Missouri Research Reactor HEU Fuel Plates

prepared by
Guanyi Wang[1], Firat Cetinbas[1], Walid Mohamed[1], Gerardo Aliberti [1], Dhongik S. Yoon[1], Yeon Soo Kim[1], Valerio Mascolino[1], Maria Pinilla[2], Erik H. Wilson[1]

[1]Nuclear Science & Engineering Division, Argonne National Laboratory
[2]University of Missouri Research Reactor

September 2024

(This page left intentionally blank)

Executive Summary

The University of Missouri Research Reactor (MURR) located in Columbia, Missouri is one of six U.S. High Performance Research Reactors (USHPRR), including one critical facility, that is actively collaborating with U. S. Department of Energy (DOE) National Nuclear Security Administration (NNSA) Material Management and Minimization (M3) Office of Reactor Conversion and Uranium Supply to convert from the use of highly enriched uranium (HEU; ⩾20 wt% U-235) to low-enriched uranium (LEU; <20 wt% U-235) fuel. A new type of very high-density LEU fuel based on an alloy of uranium and 10 wt% molybdenum (U-10Mo) is expected to allow the conversion to LEU of MURR, as well as four other USHPRR.

MURR has been working with the NNSA M3 USHPRR Project Reactor Conversion Pillar to perform fuel element design and fuel cycle performance analyses, steady-state thermal hydraulics safety analyses, and accident safety analyses in preparation for the conversion of MURR. The U-10Mo LEU fuel is currently undergoing irradiation and post-irradiation testing under a planned and documented fuel qualification effort to document properties and fuel element performance data to qualify the fuel for use in research reactors. Mini-plate and large-size plate irradiations have been successfully performed by the FQ Pillar, and more irradiation experiments are either ongoing or planned.

In order to support comparative thermal hydraulic analyses of both HEU and LEU MURR cores, irradiation thermo-mechanical analysis of an HEU plate and coolant channel have been completed. The modeling approach is consistent with the previous LEU analysis, with all relevant geometry information, neutronics data, TH inputs, and properties updated for the HEU fuel and core conditions.

Three-dimensional finite element (FE) models were developed to analyze the irradiation T-M behavior of the outermost fuel plate in MURR HEU fuel element (plate 24). This work focused on the development of material models for the HEU fuel system and the prediction of coolant channel reduction due to the irradiation T-M effects. Regarding the fuel properties, for those used in the HEU safety analyses (e.g., thermal conductivity, heat capacity), consistent values are adopted in this work. For other fuel properties required for this work but not used in prior HEU analysis, a literature survey, and sensitivity analysis, was performed.

The outcome of this work showed that reduction in the outermost coolant channel (channel 25) thickness in MURR HEU fuel element has a maximum stripe-averaged value of 20.1 mil, which occurs at middle-of-life elements (at 1409 hr of irradiation). This is comparable to the reduction in channel 24 in the MURR LEU element (20.6 mil, occurring at end-of-life elements) based on the plate-level irradiation T-M analysis of the MURR LEU plate 23.

Overall, these thermo-mechanical analyses predict smaller gap thickness redcution in previously limiting regions. Larger reductions are predicted in the middle of channels, especially for end channels where power density is not typically a maximum. An additional thermo-mechanical analysis was performed for the outermost HEU fuel plate, which showed a similar magnitude of deflection as the outermost LEU plate. At the beginning-of-life (BOL), with only thermal loads, a maximum stripe-averaged coolant channel reduction of 16.5 mil is predicted. This value is only 18% less than the all-time peak value of 20.1 mil, indicating that thermal expansion plays a significant role in the outward displacement of MURR HEU plate 24 under the employed mechanical constraint assumptions. This is in the same order of magnitude compared to the LEU plate-level model results. Thermal hydraulics analyses for HEU core have been completed in a separate work to evaluate the impact for the MURR HEU core and show that MURR maintains thermal hydraulic margins.

Table of Contents

List of Figures

List of Tables

1 Introduction

As part of the U.S. Department of Energy (DOE) National Nuclear Security Administration (NNSA) mission to eliminate or minimize the civilian use of highly enriched uranium fuel (HEU, ≥ 20 wt% U-235), the NNSA M3 Reactor Conversion and Uranium Supply Program is actively collaborating with stakeholders to convert six domestic U.S. High Performance Research Reactors (USHPRR), including one critical facility, to the use of low-enriched uranium (LEU, < 20 wt% U-235) fuel. These USHPRR still use and regularly refuel with HEU fuel. The activities that will result in the conversion of the USHPRR are being led by the following USHPRR Project's four pillar organizations, each of which is responsible for a specific aspect of the USHPRR conversion effort [1]:

- Fuel Qualification (FQ) Pillar: Design and execute the test and fuel qualification irradiation campaigns; characterize and document the fuel performance and properties; prepare reports of the tested fuel system for submission through the relevant regulators.
- Fuel Fabrication (FF) Pillar: Deploy viable industrial processes for the commercial production of LEU fuel elements for the six facilities under the scope of the USHPRR Project.
- Reactor Conversion (RC) Pillar: Perform with the facilities all the necessary activities to convert the reactors such as fuel element design, reactor core safety analysis, licensing or other regulatory submittals and implementation.
- Cross-Cutting (CC) Pillar: Address cross-pillar activities including, but not limited to, fuel transport and back-end planning.

A new type of LEU fuel with very high density, based on an alloy of uranium and 10 weight percent molybdenum (U-10Mo), is expected to allow the conversion to LEU of USHPRR that are not planned to be converted with uranium silicide-aluminum (U_3Si_2-Al) dispersion fuel [1].

The University of Missouri Research Reactor (MURR), located in Columbia, Missouri, is one of the USHPRR. Each of the MURR HEU fuel elements have 24 curved fuel plates. The number of elements loaded on the core grid plate is fixed at eight, since each element fills 45° of the annular reactor core. MURR is operated on a weekly schedule with extremely high utilization (a 92% capacity factor is typical). To maintain the same flux profile during each cycle, cores are composed of four pairs of elements at different burnup states so that the average fuel element burnup of the core is the same from week to week. Each fuel element is generally shuffled 18–20 times during its lifetime to utilize the uranium in the elements and to control power peaking. MURR typically consumes about 22 HEU elements per year at 10 MW operation.

MURR has been working with the RC Pillar team at Argonne National Laboratory to perform fuel element design and fuel cycle performance analyses, steady-state thermal hydraulics (TH) safety analyses, and accident safety analyses in preparation for the conversion of MURR. A power increase from 10 MW to 12 MW was proposed for the conversion from HEU fuel to LEU fuel [2]. The preliminary Safety Analysis Report (SAR) for conversion to LEU fuel was completed, and a detailed description of the preliminary MURR LEU fuel element design can be found in [3]. Performance and safety analyses have also been completed, which demonstrate satisfactory experimental performance and margins to safety for HEU and the preliminary LEU fuel element design following a major facility upgrade [4]. The planning and safety analysis for the sequence of transition cores following conversion from HEU to equilibrium LEU operations has been also completed [2].

The preliminary LEU fuel element design has 23 curved fuel plates with a fuel core made of the monolithic U-10Mo alloy that is currently being qualified for the conversion of USHPRR by the FQ Pillar at Idaho National Laboratory. The current HEU fuel element consists of 24 curved fuel plates with a uranium aluminide dispersion fuel meat.

Subsequent to the preliminary design stage and in preparation for later safety analyses, the RC Pillar is completing additional structural evaluations as a part of detailed design. Compared to the HEU element, several changes have been made in LEU element design to match the operational and performance requirements of the reactor after conversion. For instance, the LEU element will have 23 LEU fuel plates instead of 24 HEU plates. In addition, the LEU plates, with denser fuel cores, will be thinner compared to HEU. The differences in MURR LEU plates and element design (compared to HEU) are significant enough that the conversion safety analysis requires structural behavior to be evaluated. Furthermore, NUREG-1537 requirements indicate that mechanical forces and stresses, hydraulic forces, deformation, thermo-mechanical (T-M) changes and temperature gradients, fluid-structure interaction, and irradiation performance (e.g., fuel swelling, irradiation creep, etc.) in the fuel plates and element are to be evaluated [5, 6]. An initial evaluation of the structural behavior for LEU plate 23 was completed and showed significant displacements that require further analysis [7]. Further investigation indicated that the outer end coolant channel gap assumed for MURR LEU steady-state operations and accident analyses in [4, 8] remained reasonable, but that the channel reduction in the middle of the plate, and in the outer end channel, which are typically less limiting due to lower power, may cause those locations to be limiting. Subsequent finite element analysis (FEA) was performed to model and simulate the irradiation T-M response of selected MURR LEU fuel plates under typical irradiation conditions for the proposed MURR LEU fuel core [8].

TH impacts of the predicted coolant channel reduction from irradiation T-M model for the MURR LEU core are being evaluated and a comparison to those for the MURR HEU core is also anticipated to be needed in support of conversion and licensing. Therefore, in this work, the irradiation T-M analysis of MURR HEU fuel plate was performed to be compared with the irradiation T-M analysis results of the MURR LEU plate [8]. The modeling approach is consistent with the previous LEU analysis, with all relevant geometry information, neutronics data, TH inputs, material properties and behavioral models updated for the HEU fuel and core conditions. Model development was performed using COMSOL Multiphysics 6.1 software [9]. The outmost fuel plate of the HEU element, plate 24, was analyzed to evaluate the outmost coolant channel gap reduction for the HEU core.

2 Model Development

2.1 MURR HEU fuel

MURR switched to using a uranium-aluminide dispersion UAl_x fuel material with a maximum loading of 775 g of U-235 per element in 1971 [10]. Before this conversion, a uranium-aluminum alloy fuel with each element loaded up to 650 g of U-235 was used since the initial startup [10]. The UAl_x-Al dispersion fuel plate consists of fuel meat and cladding. The cladding is made of AA6061, and the fuel meat includes the UAl_x fuel powder and the Al matrix. The excellent performance of aluminide UAl_x fuels has been consistently demonstrated over the past decades in test and research reactors such as the ATR and the MURR. MURR has used more than 900 UAl_x fuel elements since 1971 with no failures [10].

A summary of the MURR HEU fuel element description is provided in Table 2.1. The fuel plate thickness is 0.050 inch, with the fuel meat thickness of 0.020 inch and cladding thickness of 0.015 inch on each side of the fuel meat.

Table 2.1. Summary sheet for MURR HEU fuel element [10].

Description	Value
Type of fuel	Aluminide-UAl_x, mostly UAl_3 phase
Fuel density (U-235 loaded per cubic centimeter)	1.5 – 1.6 g/cm^3
U-235 enrichment	93%
Fuel meat thickness	0.020 inch
Cladding thickness	0.015 inch
Number of fuel plates	24
Fuel plate thickness	0.050 inch
Overall fuel plate length	25.5 inch
Overall fueled length	24 inch
Internal channel gap thickness	0.080 inch
End channel gap thickness [11]	0.110 inch for channel 1 and 0.090 inch for channel 25

2.2 Geometry

The MURR HEU fuel element consists of 24 arc-shaped fuel plates, as shown in Figure 2.1. The arc angle of these fuel plates is about 45°. A comb is attached over the fuel plates at their top and bottom sides to provide additional structural support and help maintain fuel plate spacing. In addition, top and bottom end fittings are attached to the side plates using rivets.

In the previous T-M analysis for MURR LEU plates [8], it was found that the fuel plate deflects outwards due to the combined effects from thermal expansion, swelling, irradiation creep, and mechanical constraints. MURR LEU plate-level T-M model predicts a 21-mil stripe-averaged channel gap reduction for the outermost end channel (channel 24) and only 2-mil stripe-averaged channel gap reduction for the internal channel between plate 22 and 24 (channel 23). This is because the two fuel plates deflects outward in a similar way, and the change in channel 23 thickness is due to the relative displacement of plates 22 and 23. For the HEU fuel element, a similar difference between the inner and outer channel reductions is expected.

Therefore, this T-M analysis focused on the outermost plate 24 of the HEU element. Figure 2.2 is the cross section of a typical MURR fuel plate. The corresponding dimensions for the MURR HEU plate 24 are listed in Table 2.2.

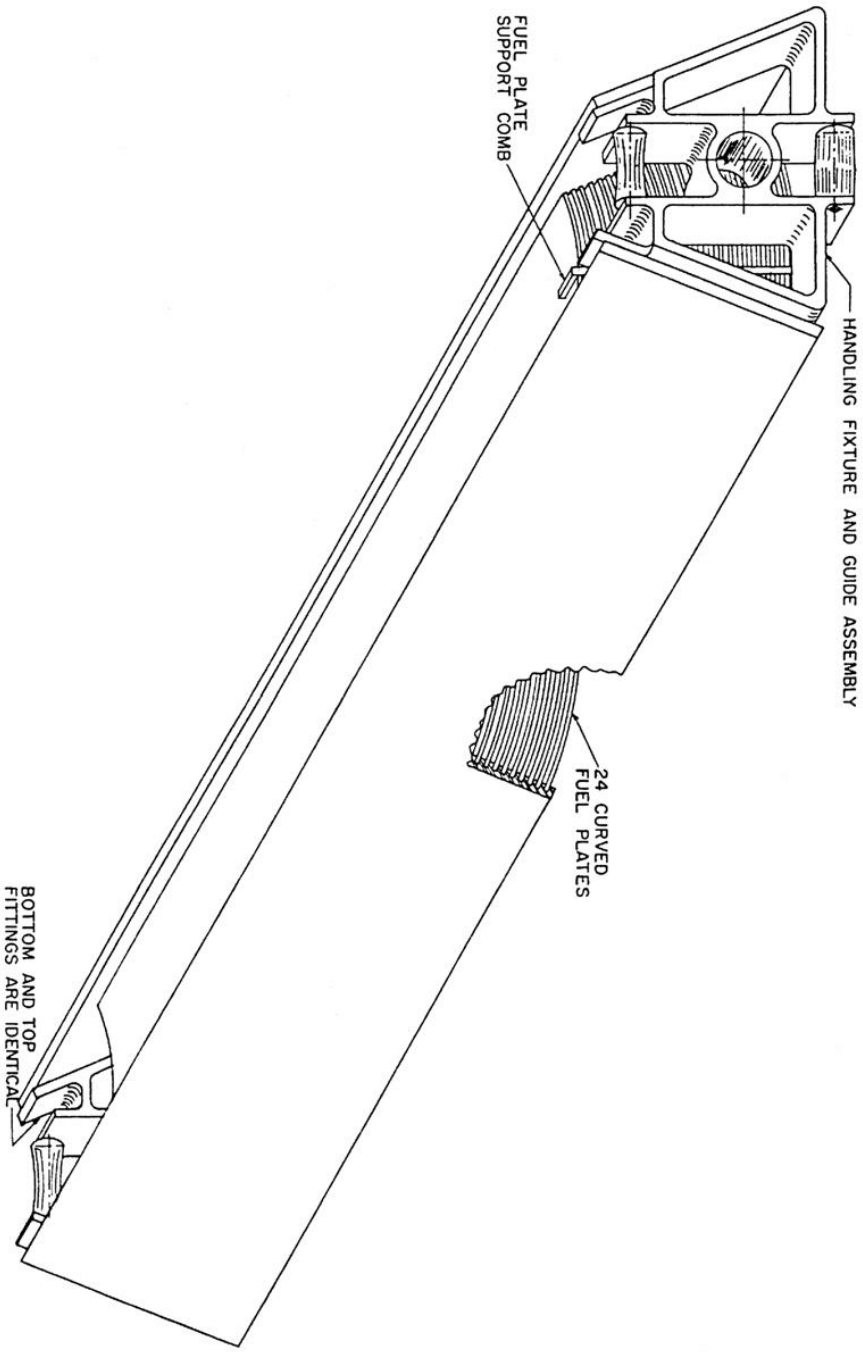

Figure 2.1. MURR HEU fuel element [10].

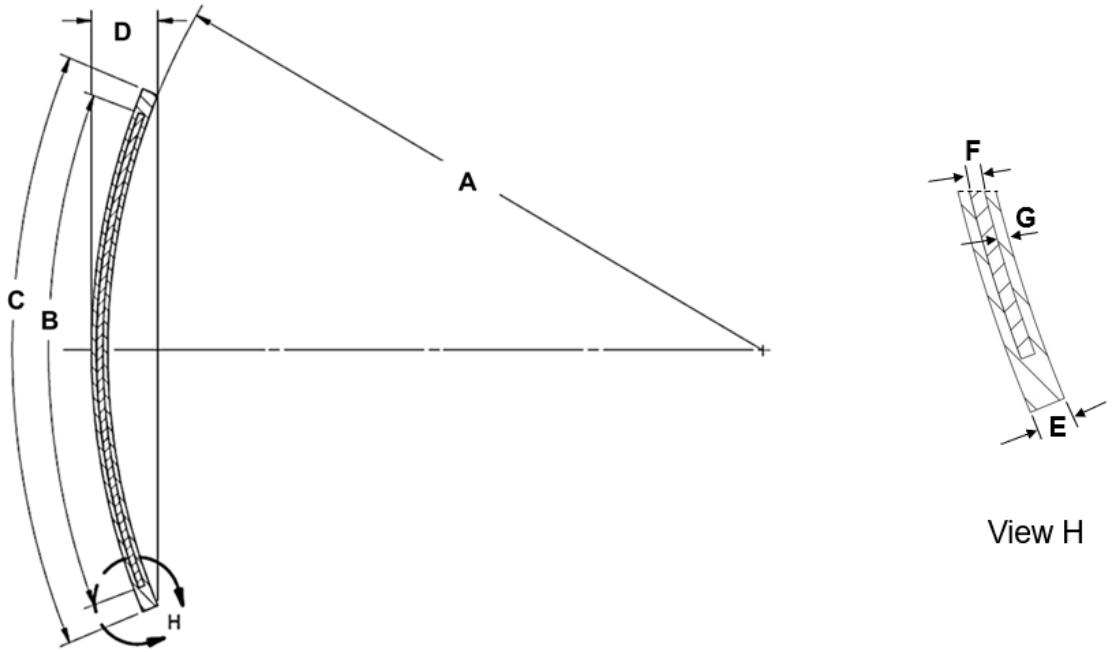

Figure 2.2. Cross section of a typical MURR fuel plate.

Table 2.2. Fuel plate 24 dimensions corresponding to Figure 2.2.

Dimensions in Figure 2.2	Dimension Explanation	Plate 24, inch
A	Radius of curvature for inner surface	5.76
B	Fuel width: arc length at the plate center in thickness direction	4.052
C	Plate width: arc length at the plate center in thickness direction	4.342
E	Plate thickness	0.050
F	Fuel meat thickness	0.020
G	Cladding thickness	0.015

2.3 Modeling Approach

As shown in Figure 2.3, the UAl_x-Al dispersion fuel plate consists of fuel meat and cladding. The cladding is made of AA6061, and the fuel meat includes the UAl_x (mostly UAl_3) fuel powder and the Al matrix.

The focus of this work is the plate displacement due to thermal load and irradiation effects; thus, the interaction and stresses between the UAl_x fuel powder and the Al matrix are not considered. The overall plate displacement can be predicted reasonably well by assuming a homogenized fuel meat domain if the fuel meat material properties and behavior models are properly given. In addition, swelling models of UAl_x-Al dispersion fuel usually provide volumetric change rate for the fuel meat, instead of UAl_x powders, which even makes it preferable to model the fuel meat as the homogenized domain instead of particles. In this work, the fuel meat is analyzed by assuming a homogenized domain and considering the material properties and irradiation effects for the mixture, as shown in

Figure 2.3. A detailed review of the material properties of UAl_x, Al, and their mixture will be discussed in Section 3. Also, ideal bonding was assumed at the cladding-cladding and cladding-fuel meat interfaces, thus, delamination at these interfaces is not permitted.

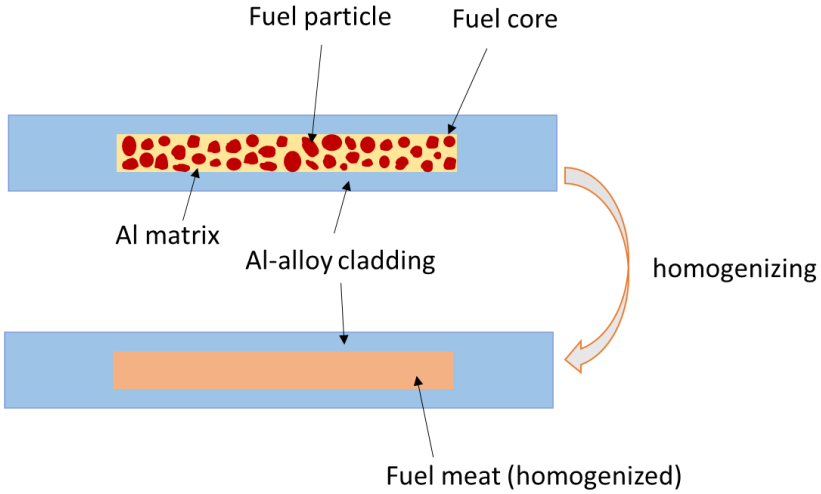

Figure 2.3. Schematic of the HEU fuel composition and the homogenization approach.

2.4 Irradiation Conditions

There are eight positions for the fuel elements in the MURR core, labeled as X1 through X8. The fuel elements in these positions are typically loaded in four pairs with similar burnup. Based on typical burnup levels for the elements loaded in the core, the elements have been modeled in previous work as low burnup (X1/X5), low-moderate burnup (X3/X7), high-moderate burnup (X2/X6), and high burnup (X4/X8) [2]. It should be noted that the burnup levels and corresponding element position pairs are based on the work presented in [2], and may be affected by possible changes in MURR fuel management. In this work, the total irradiation time of 2873 hours to reach the typical discharge burnup for an element was divided into four steps, based on the irradiation history of these elements, as follows: (1) Irradiation-1 until 48 hours to achieve equilibrium xenon conditions; (2) Irradiation-2 of length 1361 hours, from 48 hours to 1409 hours; (3) Irradiation-3 of length 151 hours, from 1409 hours to 1560 hours; and (4) Irradiation-4 of length 1313, from 1560 hours to 2873 hours.

The FE model developed in this work simulated a steady-state heating step followed by 4 consecutive transient irradiation intervals as outlined above. The fission density, power density, and the fast neutron fluence data at the end of each irradiation interval were obtained from the neutronics calculations, and linear interpolation was used in the T-M model during each irradiation interval. These inputs are discussed in detail in the Section 2.4.1.

During irradiation, the heat generated in the fuel meat is removed by the coolant. The FE model was developed to solve the temperature field within the fuel plate, whereas the coolant temperature field was considered as a known model input from an independent TH analysis. The heat removal by the coolant was modeled with convective boundary conditions on the cladding surfaces in contact with the coolant. A constant coolant temperature and heat transfer coefficient were used. The coolant conditions as model inputs are discussed in Section 2.4.2.

2.4.1 Neutronics Data

Two-dimensional (2D) distributions of power and fission densities for the previously mentioned irradiation intervals were obtained with the MCNP5 v1.60 software [12] and used as direct inputs to the FE model. The adopted 2D neutronics grid covers only the fueled section of the plate. The fuel meat length was resolved with 24 equidistant nodes, while the fuel meat width was discretized into a total of 9 nodes with 5-mm-wide edge stripes (three on each side for a total of 6 stripes) and 3 central stripes of equal width (see Figure 2.4 for the planes used for the azimuthal partitioning of the fuel meat in the neutronic model). The spatial discretization in the FE model was significantly finer than the neutronics grid. Therefore, the FE model assumed linear interpolation between the node centers of the neutronics grid.

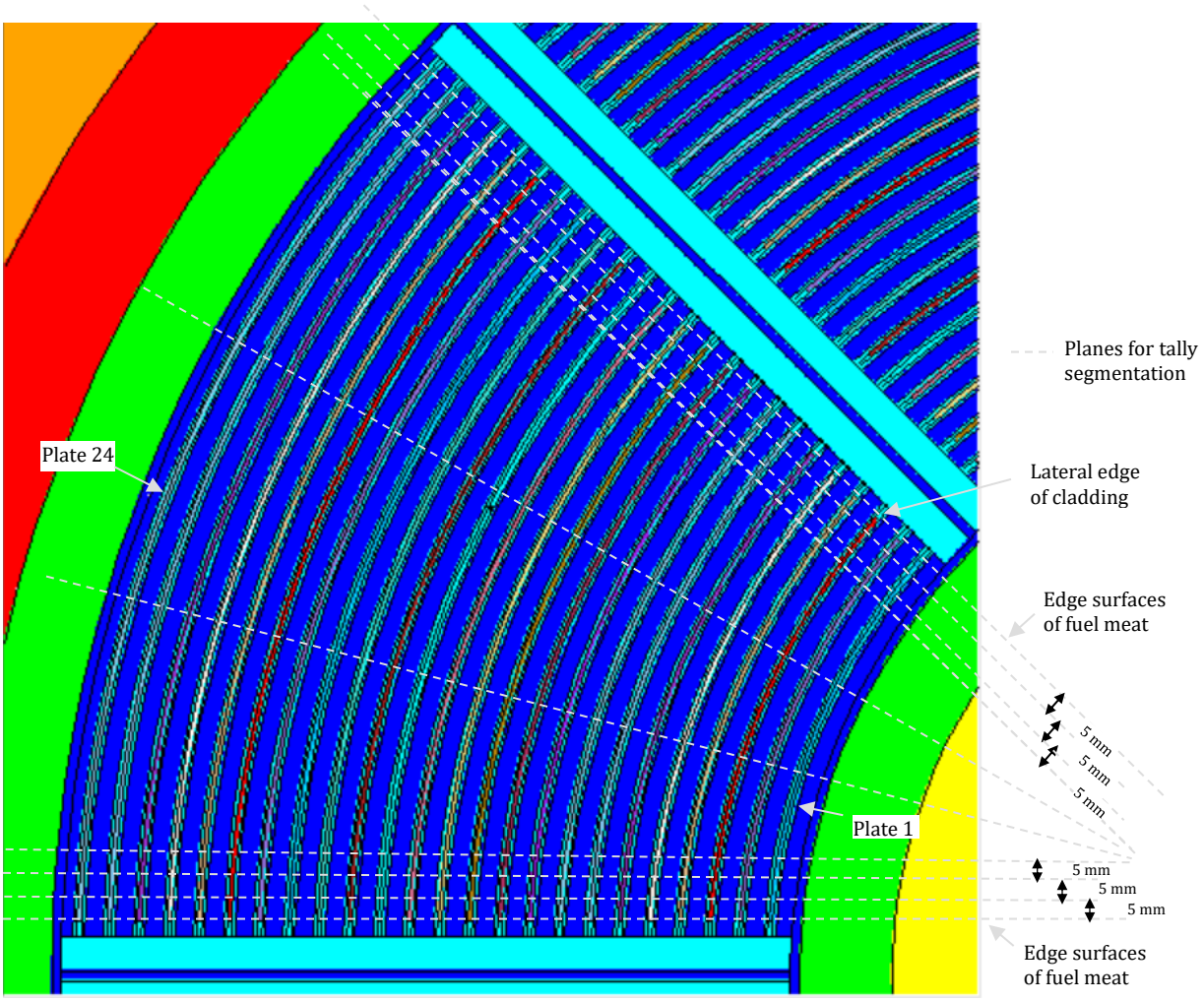

Figure 2.4. Schematic view of the azimuthal planes used for the partitioning of the power tallies.

In the present analysis, the plate power density profile over the life of a typical HEU element was derived from the power distributions from the prototypic HEU core with equilibrium xenon conditions. The adopted model used the experimental facility and loading conditions that were typical of the MURR operation in 2018. For the calculation, it was assumed that the average power

density of the elements with similar burnup in the core is representative of the power density in a typical MURR HEU element after the corresponding irradiation time. More in detail:

- The average power density of elements in position X1 and X5 was assumed to be representative of the power density in a typical HEU element after 48 hours of irradiation (these elements are in their 1st cycle of use in the prototypic fuel cycle simulation).
- The average power density of elements in position X3 and X7 was assumed to be representative of the power density in a typical HEU element after 1409 hours of irradiation (these elements are in their 10th cycle of use in the fuel cycle simulation).
- The average power density of elements in position X2 and X6 was assumed to be representative of the power density in a typical HEU element after 1560 hours of irradiation (these elements are in their 11th cycle of use in the fuel cycle simulation).
- The average power density of elements in position X4 and X8 was assumed to be representative of the power density in a typical HEU element after 2873 hours of irradiation (these elements are in their 19th and final cycle of use in the fuel cycle simulation).

The plate fission density profiles at each time point in the FE model were calculated by integrating the power density in each of the 24 × 9 nodes in the fuel plate over the irradiation interval and dividing by a recoverable energy of 198.36 MeV [13] per fission. To normalize the nominal reactor power, the sum of all tally values (the f7 tally was used in the MCNP calculation) was scaled to a total value of 10 MW. Figure 2.5 and Figure 2.6 show the calculated power and fission density profiles in plate 24 for each irradiation interval discussed above.

Fast neutron (E > 0.1 MeV) fluence calculations were performed in the meat, cladding, and side plates of a typical MURR element at the selected irradiation times of the FE model. For the fast fluence data, detailed flux distributions were obtained for the element loaded in position X1 of the same HEU core used for the power and fission density calculations. In a conservative approach, the fast fluence data were calculated with the assumption that the fast flux distributions of the element in position X1 are constant during the lifetime of the typical HEU element. For the side plates, flux and fast fluence data were calculated in 28 axial meshes (the 24 axial meshes of the fuel meat plus two additional meshes for the portion of the side plates extending above and below the fuel meat). For the cladding, results were obtained in 11 azimuthal stripes (9 stripes consistent with the azimuthal discretization of the meat plus one additional stripe for each lateral edge of the cladding) and 26 axial meshes (the 24 axial meshes of the fuel meat plus one additional mesh for the cladding above and below the fuel meat) for each plate. In the fuel meat, flux and fast fluence data were calculated in nine azimuthal stripes and 24 axial meshes. Spatially averaged flux values were obtained for the cladding on the lateral surfaces of the meat. Fluxes were tallied in three energy bins, with energy below 0.1 MeV, above 0.1 MeV (fast fluxes) and in the total energy domain. The cumulative fast neutron fluence of plate 24 at the end of each irradiation interval is listed in Table 2.3. The averaged values in Table 2.3 do not include the fast fluence in lateral edge of the cladding.

Table 2.3. Cumulative average fast neutron (E > 0.1 MeV) fluence (neutrons/m^2) in cladding for plate 24.

Irradiation Time, hr	Cumulative average fast neutron fluence, (neutrons/m^2)
48	3.37×10^{23}
1409	9.89×10^{24}
1560	1.09×10^{25}
2873 (end-of-life; EOL)	2.02×10^{25}

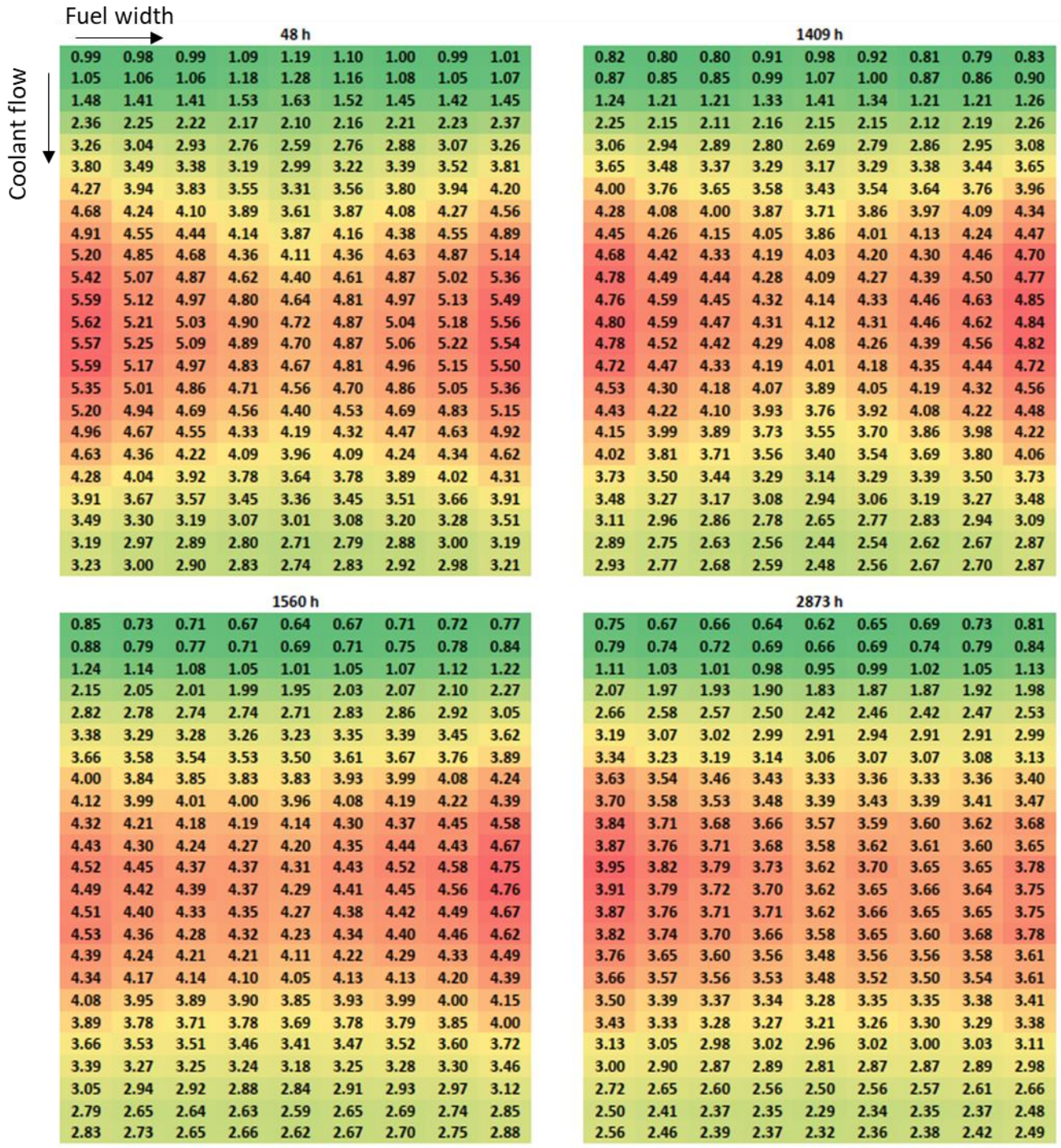

Figure 2.5. Plate 24 power density (kW/cm³) distribution on the neutronics grid for each irradiation interval.

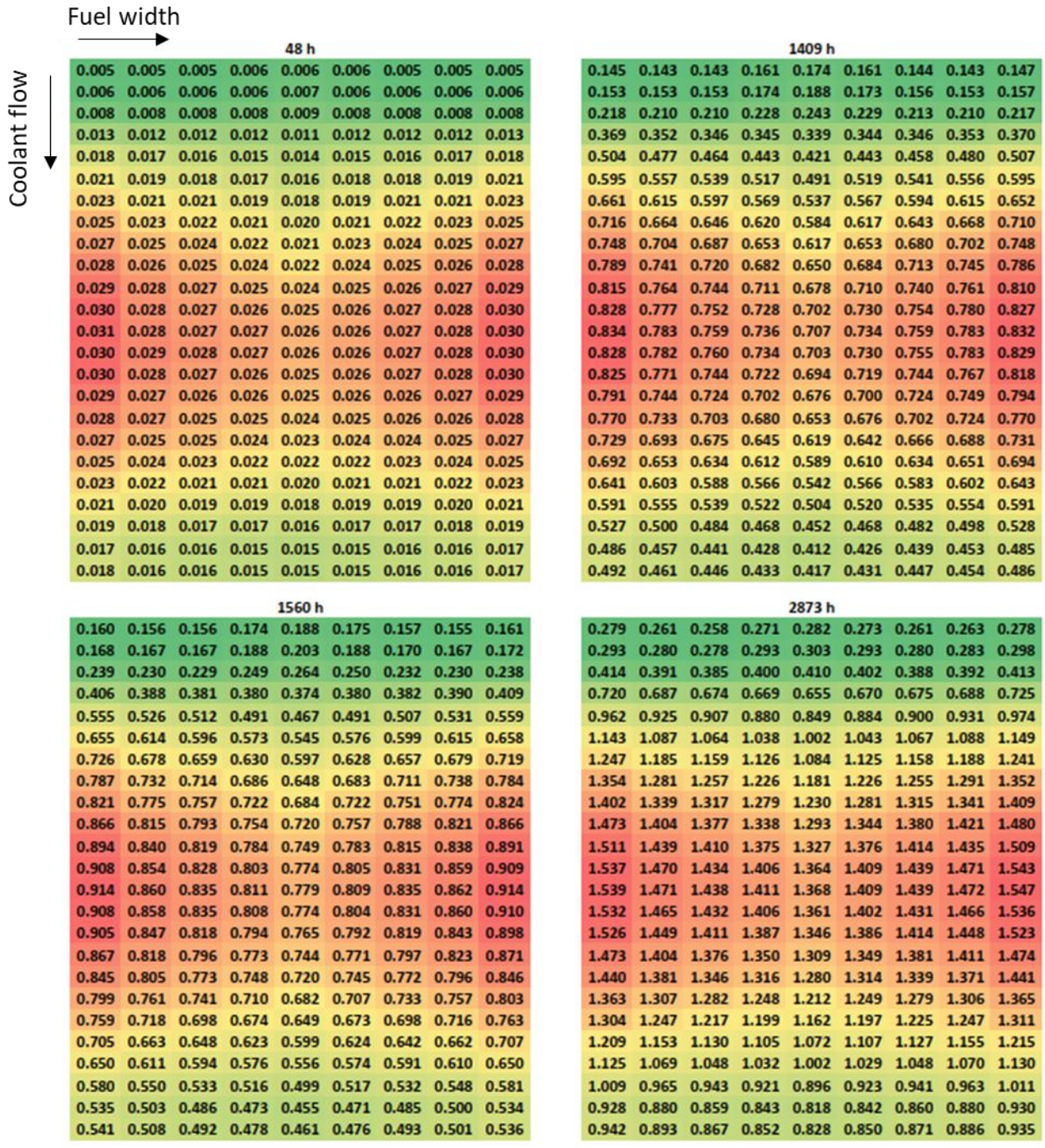

Figure 2.6. Plate 24 fission density (10^{21} fissions/cm^3) distribution on the neutronics grid for each irradiation interval.

2.4.2 Thermal Hydraulics Data

The FE model employed coolant temperatures and heat transfer coefficients (HTC) from the prototypic MURR HEU operation as boundary conditions at the plate surfaces. The coolant temperature and HTC were obtained using PLTEMP/ANL v4.3 [14] from the existing full-core model for the MURR HEU core [3, 4]. The TH analysis provided a 2D map of coolant temperature and HTC

distribution on a grid over the fueled section of the plate (same as the grid for the neutronics data). The FE model conservatively employed a one-dimensional (1D) distribution of the coolant temperature and the HTC in the axial (fuel length) direction from the hottest stripe in the TH analysis. TH data on the 24 equidistant nodes on the fuel length was mapped onto the FE grid, assuming linear interpolation between the node centers and constant extrapolation to the unfueled length of the plate. Both the coolant temperatures and the HTC were assumed to remain constant with time during the entire irradiation history.

The existing PLTEMP/ANL model includes various hot channel factors (HCFs) to account for manufacturing and calculational uncertainties and channel gap reduction due to burnup-related effects. The model was updated to be the best estimate to obtain the coolant conditions for the baseline FE model of the MURR HEU plates. This means that the TH calculations were performed based on the nominal core geometry and conditions and without accounting for any manufacturing and calculational uncertainties. The best estimate coolant conditions were used for the baseline FE model because the FEA is intended to provide the best estimate channel gap reduction and to maintain the same approach as the irradiation thermo-mechanical modeling of MURR LEU plates [8].

As will be discussed in Section 4.2, sensitivity analysis was performed to assess the impacts of variations in the coolant conditions. The sensitivity of the predicted channel gap reduction was evaluated with the coolant conditions obtained using some HCFs used for the safety analysis as well as accounting for the channel gap reduction due to burnup-related effects. Table 2.4 outlines a set of HCFs used for the sensitivity analysis. More details on the assumptions employed to obtain the numerical values for these HCFs can be found in [11]. It is noted that the channel gap reduction due to burnup-related effects assumed for the HEU relicensing was used for this sensitivity analysis. As will be shown in Section 4.2, the channel 25 gap reduction predicted by this irradiation T-M analysis is not sensitive to the use of HCFs, including the ones from the channel gap reduction due to burnup-related effects.

Table 2.4. List of HCFs and their values used to generate inputs for the FE model.

Hot channel factor	Values
Local fuel homogeneity	20%
Stripe fuel homogeneity	1%
Flow mal-distribution	15%
Channel gap tolerance (fabrication)	8 mil (interior channels) 4 mil (outer channels)
Channel gap reduction due to burnup-related effects	10 mil (interior channels) 5 mil (outer channels)

2.5 Mechanical Constraints and Boundary Conditions

The side plates along the length of the MURR HEU element provide mechanical support and hold the fuel plates in place within the grooves. The fuel plates are connected to the side plate grooves through a swaging joint. In this plate-level T-M analysis, neither the side plates nor the grooves were explicitly modeled. It was conservatively assumed that the side plates are rigid, and the swaging is perfect in a way that prevents the motion of the fuel plates in all directions. The rigid side plates with perfect swaging connections were addressed through mechanical constraints applied to the fuel plates. As illustrated in Figure 2.7, the surfaces of the simulated MURR HEU fuel plate 24 in contact with the side plate grooves (in green) were constrained in all directions.

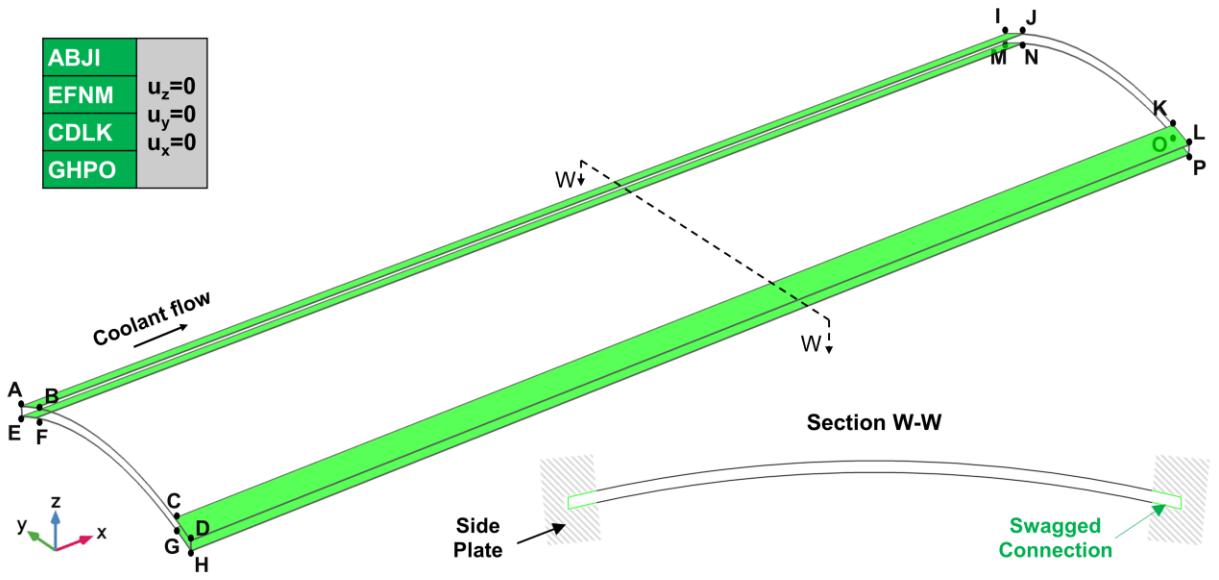

Figure 2.7. Fuel plate mechanical constraints employed in the FE models.

The FE model did not explicitly model the fluid domain, and the heat flux from the fuel plate to the coolant was addressed using boundary conditions based on the coolant temperature and HTC distribution obtained from the TH analysis described in Section 2.4.2. On the surfaces BCKJ and FGON, the following convective heat flux condition was assigned:

$$-k\frac{\partial T}{\partial n} = h(T - T_b) \tag{1}$$

where T is temperature, k is the thermal conductivity, n is the surface normal direction, h is the convective heat transfer coefficient (HTC) and T_b is the bulk coolant temperature. The axial distribution of the coolant temperature and HTC are presented in section 4.2.

2.6 Numerical Approach

The MURR HEU fuel plate 24 was modeled using the commercial FE software COMSOL Multiphysics 6.1 [9]. The solid mechanics and heat transfer equations were discretized using second-order serendipity and Lagrange elements, respectively. The highly nonlinear and coupled system of solid mechanics and heat transfer equations was solved using a segregated approach. The system was linearized through the so-called Newton iterations, and the linear systems of equations were solved with the direct solver PARDISO which is one of multiple solvers that are part of the COMSOL software [9]. Implicit time stepping using a backward differentiation formula (BDF) was adopted, which was the default option of the software.

A sensitivity analysis was performed regarding the geometric nonlinearity, and the results show that including the geometric nonlinearity model has a negligible impact on the maximum displacement (reducing it by less than 1 mil). Therefore, geometric nonlinearity was not considered in this work, following the same approach used in the MURR LEU T-M analysis [8].

A structured mesh scheme was used for spatial discretization of the fuel plate. The in-plane (i.e., the convex surface) geometry was meshed using quadrilateral elements and swept through the thickness

of the plate. A mesh sensitivity study determining the in-plane mesh size and the number of elements in each layer is presented in Appendix A.

As shown in Figure 2.8, the optimized mesh consists of four layers in the entire thickness of the fuel meat, and two layers in the AA6061 cladding on each side. The unfueled portions of the fuel plate consist of eight layers of AA6061. The total number of elements in the plate was ~49k and ~1.1M degrees of freedom (DOF) with an additional ~9.2M internal DOF were solved for the irradiation intervals.

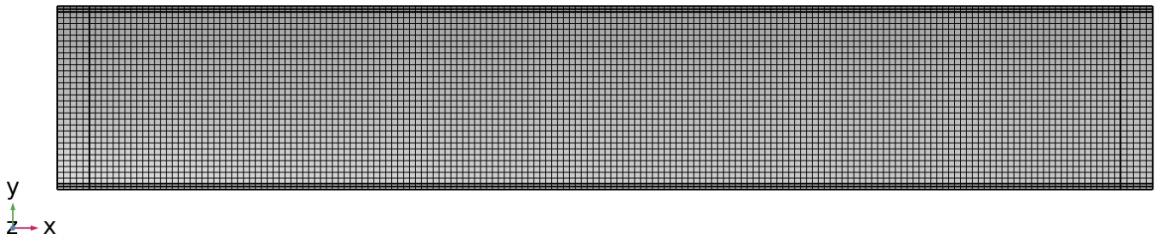

(a) In-plane mesh

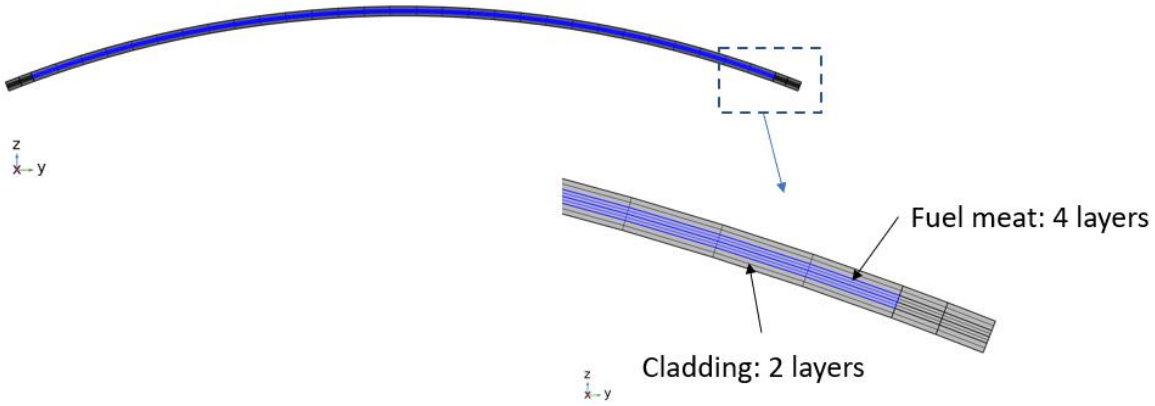

(b) Through-thickness mesh

Figure 2.8. Mesh used in the FE models.

3 Material Properties and Behavior Models

3.1 UAl_x-Al Fuel Meat

Typical UAl_x powder consists of about 6 wt% UAl_2, 61 wt% UAl_3, and 31 wt% UAl_4 [15]. During the plate fabrication process, almost all UAl_2 reacts with the aluminum matrix to form UAl_3, and some UAl_3 reacts with aluminum to form UAl_4 [15]. The exact fractions of the compounds included in UAl_x depend on the fabrication process set by the fuel fabricator. It was assumed that the UAl_x in the fuel meat of the finished plate consists of 60 wt% UAl_3, and 40 wt% UAl_4 in the research reactor conversion guidebook [15], and the same assumption on the UAl_x composition is used in this work.

3.1.1 Density

The density of UAl_3 and UAl_4 is 6.8 g/cm^3 and 5.7 g/cm^3, respectively [15]. So, the density of the UAl_x compounds with 60 wt% UAl_3 and 40 wt% UAl_4 is 6.36 g/cm^3. The density of Al is 2.7 g/cm^3 [16]. Note that a small amount of porosity exists in the fuel meat during the fuel fabrication, and a typical value of 7 vol% [15] is assumed here. Using the nominal fuel loading of 775 g U-235 (1.5-1.6 g U-235/cc) [10] in the MURR HEU element, the UAl_x vol% of the fuel meat is calculated to be 34.3%. Therefore, the density of the UAl_x-Al fuel meat is 3.77 g/cm^3.

Note that 3.77 g/cm^3 is the density of unirradiated fuel at room temperature. The thermal expansion coefficient and the swelling correlation, which will be discussed later in this section, are used to calculate the fuel meat density of the irradiated material at elevated temperatures.

3.1.2 Thermal Conductivity

To provide the technical basis for support of the conversion of MURR from HEU to LEU, steady-state TH analysis had been performed for both the MURR HEU core and LEU core [11]. For this work, the thermal conductivity of the fresh HEU fuel meat of 40 W/(m·K) was used based on the data provided in Table 4 and Figure 8 of the research reactor conversion guidebook [15]. Also, the value at maximum burnup of the MURR HEU fuel was assumed to be 30 W/(m·K) based on engineering judgment considering the degradation of fuel meat thermal conductivity due to irradiation [11]. No other data was found in the literature for the thermal conductivity of the irradiated UAl_x–Al fuel. Therefore, the above-mentioned values were used for this T-M modeling for consistency.

3.1.3 Heat Capacity

The specific heat of UAl_x-Al can be calculated by summing the weighted specific heats of UAl_x and Al phase by their fractions [15]:

$$c_{p,UAlx-Al} = 0.892 + 0.00046\,T - W_U(0.722 + 0.00034\,T) \quad J/(g \cdot K) \tag{2}$$

where T is the temperature in °C, and W_U is the weight fraction of uranium in the fuel meat, which is calculated using equation (1) in [15] to be 40.7% using the nominal fuel loading in the MURR HEU element and an assumed porosity of 7 vol% for the fuel meat. The heat capacity of the UAl_x-Al fuel meat calculated using the above equation is listed in Table 3.1, which is used for this work. Note that the irradiation effect on the heat capacity of UAl_x-Al fuel was not considered in the prior HEU safety analysis [17] and for other fuel has not been considered as necessary [18].

Table 3.1. Heat capacity of UAl_x-Al fuel meat.

Temperature	Heat capacity	
°C	J/(g·K)	kJ/(m³·K)
20	0.605	2277
100	0.630	2374
200	0.663	2496
300	0.695	2617

3.1.4 Coefficient of Thermal Expansion

No data on the coefficient of thermal expansion (CTE) of the UAl_x-Al fuel meat is available in the literature. CTE of the aluminum-uranium alloys are provided in Table IV of Peacock and Frontroth [19], and the data is plotted in Figure 3.1. Note that the 0 Wt.% U data is from Reference [20]. The CTE of the aluminum-uranium alloy decreases as the wt% of U in the alloy increases. In addition, Mei and Yacout [21] performed a first-principle study of the structural properties of uranium aluminides, and the CTE of UAl_3 are calculated as plotted in Figure 3.1. For the comparison with the aluminum-uranium alloy data, the wt% of U is 74.4% in UAl_3.

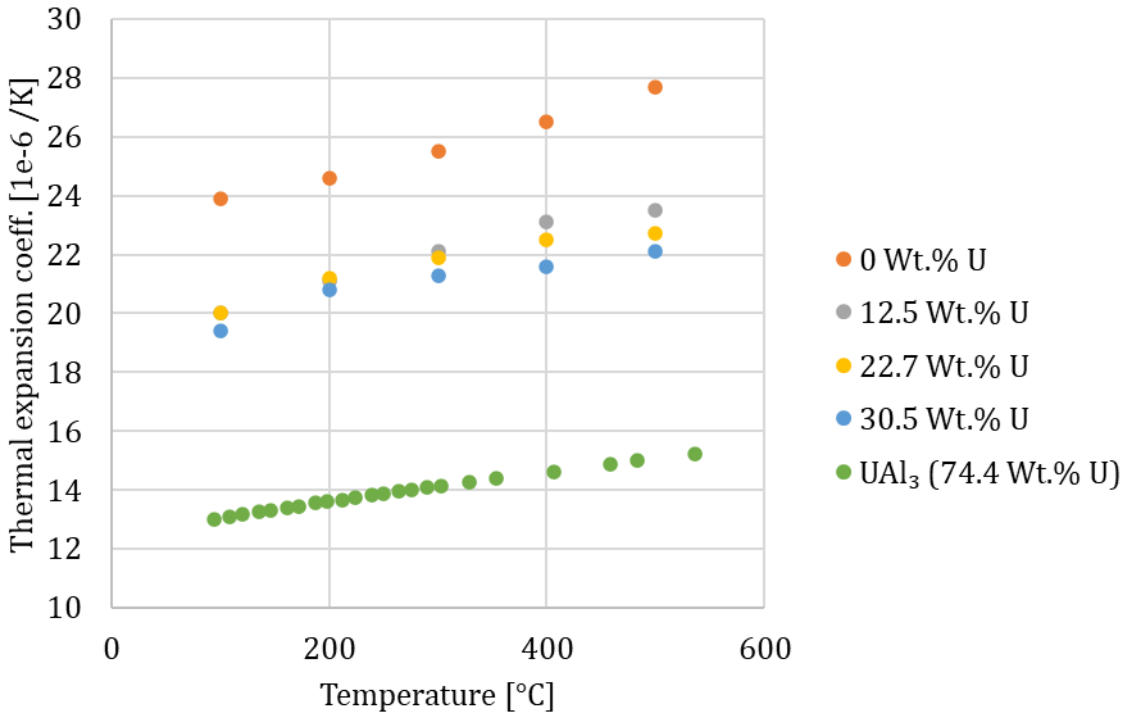

Figure 3.1 Measured CTE data of aluminum-uranium alloys [19] and calculated CTE of UAl_3 [21] UAl_3 is 74.4 wt% U.

It is expected that the CTE of the UAl_x-Al fuel meat is bounded by the values of UAl_3 and Al (0 wt% U). Therefore, the CTE of both UAl_3 and Al will be used in the simulation to evaluate the sensitivity of the results to this material property. The results of the sensitivity analysis will be presented in the next section.

As mentioned earlier, the weight fraction of uranium in the fuel meat is calculated to be 40.7%, while the available data in [19] for aluminum-uranium alloys is up to 30 wt% U. For the best estimation, the CTE of aluminum-uranium alloy with 40.7 wt% U calculated by extrapolating the data in [19], is used in the simulation and listed in Table 3.2.

Table 3.2. CTE of aluminum-uranium alloys [19] and the extrapolated value for 40.7 wt% U.

Coefficient of thermal expansion (10^{-6}/K)			
wt% U Content	Temperature range (°C)		
	20-100	20-200	20-300
0	23.9	24.6	25.5
12.5%	20.0	21.1	22.1
22.7%	20.0	21.2	21.9
30.5%	19.4	20.8	21.3
40.7%	**18.6**	**20.3**	**20.5**

3.1.5 Young's Modulus

To estimate the elastic moduli of particulate composite materials, the rule of mixtures can be used [22]:

$$E_c = E_m V_m + E_p V_p \qquad \text{upper bound (linear)}, \tag{3}$$

$$E_c = \frac{E_m E_p}{E_m V_p + E_p V_m} \qquad \text{lower bound (non-linear)}, \tag{4}$$

where E is the Young's modulus, V is the volume fraction, and the subscripts m and p means matrix and particulate phases.

The Young's modulus of aluminum is around 68.3 GPa at room temperature [23]. The data for Young's modulus of UAl_x is rare. Mei and Yacout [21] predicted the Young's modulus of UAl_3 to be 164.7 GPa at room temperature. As mentioned earlier, the UAl_x vol% of the fuel meat is calculated to be 34.3%. Therefore, the upper and lower bound of the Young's modulus for the fuel meat is 84.1 GPa and 96.5 GPa, respectively.

It is expected that the Young's modulus of the UAl_x-Al fuel meat is bounded by the value of UAl_3 and Al. Therefore, the Young's modulus of both UAl_3 and Al will be used in the simulation to evaluate the sensitivity of the results on this material property. The results of the sensitivity analysis will be presented in Section 4.

Note that the sensitivity of simulation results to the elastic properties of the material like Young's modulus is low, as will be shown later. The 84.1 GPa is used in the simulation as the best-estimate case. Given that the Young's modulus of UAl_x at different temperatures is unknown, as well as the insensitivity of the model on Young's modulus, the temperature dependence is not considered in the model for the fuel meat.

3.1.6 Poisson's Ratio

The Poisson's ratio of Al is 0.33 [16], and the value of UAl_3 is 0.2 [21]. No data on Poisson's ratio of the UAl_x-Al fuel meat is available in the literature. The values for both UAl_3 and Al were used to evaluate the sensitivity of the results on the Poisson's ratio.

3.1.7 Yield Stress

The measured compressive yield stress of the unirradiated ATR type UAl_x-Al fuel was provided by Beeston et al. [24], and the values for ATR type fuel plate with 35 wt% UAl_3 are listed in Table 3.3 as these data are the most relevant and complete in terms of temperature dependence. Data for different fuel types and fuel loadings are also included in Table VI of Beeston et al. [24]. For the yield stress of irradiated UAl_x-Al fuel, the data for different types of plates are not consistent. For example, for the ATR type plate with 50 mil thickness and 51 wt% UAl_3 at 533 K, the irradiated yield strength is 82.7 MPa, which is much higher than its unirradiated yield strength of 47.3 MPa [24]. However, for the Engineering Test Reactor type plate with 50 mil thickness and 35 wt% UAl_x at 533 K, with similar fission density, the yield strength decreases from 61 MPa to 42 MPa with irradiation [24]. Note that the enrichment for all these plates is 93% [24].

Given that the effect of irradiation on the yield strength of UAl_x-Al fuel varies, sensitivity analyses were performed to evaluate the impact of yield strength on the results. These analyses are discussed in section 4.1.3.

Table 3.3. Yield stress of ATR type fuel plate, 100 mil plate thickness, 35 wt% UAl_3, unirradiated.

Temperature (°C)	Measured compressive yield strength (MPa)
94	98.5
149	91
205	81.1
260	44.8

3.1.8 Swelling

In prior analyses for the MURR HEU core [3], a coolant channel reduction of 10 mil for internal channels was used to model the effects of swelling, irradiation creep, and oxide growth. No specific swelling correlation was mentioned.

Beeston et al. [24] proposed an empirical equation based on the measured swelling data from four fuel elements and 16 samples:

$$\frac{\Delta V}{V}\% = 2.6\% \times FD/10^{21} \quad (5)$$

where $\frac{\Delta V}{V}$ is the fuel meat swelling and FD is the fission density of fuel meat in fissions/cm^3. This swelling correlation is used here.

In another report by Miller and Beeston [25], a different correlation is proposed:

$$\frac{\Delta V}{V}\% = -2.13\% + 2.37\% \times FD/10^{21} \quad (6)$$

The maximum fission density used in this analysis is around 1.5×10^{21} fissions/cm^3, as shown in Figure 2.6. The volumetric change caused by swelling at 1.5×10^{21} fissions/cm^3 is 3.9% as predicted by Equation (5) and 1.4% as predicted by Equation (6). Both correlations are used in the sensitivity analysis. The negative constant term in Equation (6) indicates an induction period for swelling equivalent to a fission density of about 1×10^{21} f/cm^3 which may occur due to initial fuel swelling being accommodated by as-fabricated porosity.

3.1.9 Irradiation and Thermal Creep

Creep is a permanent deformation that occurs over time when a material is subjected to sustained load or stress, even if the stresses are below the yield strength. It is primarily influenced by the movement of empty crystal lattice sites (vacancies), which becomes more pronounced at higher temperatures. In most cases, for metallic materials, vacancy migration is sufficient for creep when the temperature is above about 30% of the melting temperature of the material at an absolute scale (K), which is referred to as thermal creep. Irradiation creates excess point defects, which induce the irradiation creep mechanism, which supplements thermal creep and increases the overall creep rate.

No data was found on the irradiation creep of the UAl_x-Al fuel meat in the literature. The fuel meat contains 34.3 volume % UAl_x fuel particles dispersed in an aluminum matrix (the continuous phase). The majority of the fuel meat volume (58.7% Al, 34.3% fuel, and 7% porosity) is aluminum matrix. Therefore, the creep behavior of the aluminum matrix can be used to approximately represent the creep behavior of the UAl_x-Al fuel meat.

For pure aluminum, with its low melting temperature of 932 K (659 °C), 0.3 T_m is only 280 K (7 °C)[26]. Therefore, thermal creep does occur in pure aluminum at room temperature [26]. The data on irradiation creep in pure aluminum are sparse and conflicting, with one experiment showed no irradiation creep while the other showed substantial irradiation creep with enhancement factor (ratio of irradiation creep rate to thermal creep rate) of 10 to 20, as detailed by Farrell [26, 27]. One possible reason is that the irradiation was quantified in terms of neutron fluence, which depends on the facility [28]. To compare the irradiation behavior data from various facilities, displacement per atom should be used instead of fluence.

Given the uncertainties of the creep behavior model of UAl_x-Al fuel meat, sensitivity analysis will be performed on three case studies using the T-M models without creep, with thermal creep, and with irradiation creep.

The thermal creep rate can be calculated using [9]:

$$\dot{\varepsilon} = A\sigma^n \exp\left(-\frac{Q}{RT}\right) \quad (7)$$

where A is a constant, n is stress exponent, and Q is the activation energy (J/mol). These three are material-dependent parameters. σ is the equivalent stress in MPa, T is the temperature in K, and R is the gas constant (8.314 J/(mol·K)).

Matsunaga and Sato [29] reported the creep rate data for several grades of aluminum, among which 1050 Al is the commercially available 'pure' aluminum and usually used in the fuel fabrication. Using

the reported creep data for 1050 Al in [29], the A, n, and Q in the above equation can be determined to be 9.75×10^{-11} 1/s, 4, and 30 kJ/mol, respectively. These values will be used in the T-M model as the baseline for sensitivity analysis.

3.2 AA6061 Cladding

AA6061 cladding was modeled as an isotropic material accounting for elastic, plastic, thermal and swelling strains. Under typical irradiation conditions in research reactors, AA6061 swells with silicon generation and precipitation [26]. Irradiation swelling data for AA6061 as a function of fast neutron fluence was extracted from [23], as shown in Table 2.5. Instantaneous AA6061 swelling was calculated by linear interpolation in fast neutron fluence. Note that the AA6061 cladding material is more resistant to creep than pure aluminum. The creep of AA6061 cladding at typical operating temperatures of research reactors is usually insignificant and, therefore, not considered in the T-M model.

The material properties of AA6061 have been documented in detail in [23]. Since the cladding material is the same for the MURR HEU and LEU plates, the material properties and behavior models for the AA6061 cladding used in this analysis are identical to those used in the MURR LEU plate T-M model [8].

Table 2.5. Aluminum alloy (AA6061) irradiation swelling [23].

Fast neutron fluence, neutrons/m^2	Swelling, %
1.82×10^{25}	0.01
2.88×10^{26}	0.167
1.83×10^{27}	2.02

4 Model Sensitivity Analyses

The data and reference of UAl_x-Al HEU fuel physical, thermal, and mechanical properties and behavior models are limited. Therefore, extensive sensitivity analysis was performed to evaluate the impact of the fuel meat material properties and behavior models on the predicted irradiation T-M behavior of the MURR HEU fuel plate 24. The maximum displacement in the radial direction is selected as the parameter of interest because it is directly related to the channel 25 gap reduction. The four irradiation periods simulated in this work are described in section 2.4. For all the tables in this section, the selected fuel property values for the finalized model presented in Section 5 were identified as bold text.

4.1 Model Sensitivity on Fuel Meat Properties

Note that the coolant conditions (temperature and HTC) used in Section 4.1 are slightly different from those used in the finalized model. The coolant conditions used in Section 4.1 is for element X8 without HCF, but with the burnup-related coolant channel reduction considered. For the finalized model, the coolant conditions without burnup-related coolant channel reduction for element X7 and without HCF are used, which could be more representative. The impact of this difference in coolant conditions on the predicted irradiation thermo-mechanical behavior is negligible, and the difference in the predicted maximum displacement is only 0.4% (24.2 mil vs. 24.1 mil). Therefore, all the results presented in Section 4.1 is still valid to evaluate the model sensitivity on fuel meat properties.

Table 4.1 lists the fuel properties and behavior models evaluated in this section and the corresponding baseline values and models. The sensitivity is analyzed for a single property at a time and the remaining properties are kept at baseline values.

Table 4.1. Fuel meat properties and behavior models with model sensitivity evaluated and baseline value/model.

Fuel meat properties and behavior models	Baseline value/model
Young's modulus (GPa)	84.1 [21-23]
Poisson's ratio (-)	0.33 [16]
CTE (10^{-6} /K)	18.6 (temperature dependent, value listed is at 100 °C) [19]
Yield stress	N/A (Elastic only)
Creep model	1050 Al thermal creep [29]
Swelling correlation	$\frac{\Delta V}{V}\% = 2.6\% \times \frac{FD}{10^{21}}$ (Beeston et al. [24])

4.1.1 Effects of Elastic Modulus and Poisson's Ratio

Three values of Young's modulus are used in the sensitivity analysis. As detailed in Section 3.1.5, the value of 84.1 GPa is the estimated Young's modulus of the UAl_x-Al fuel meat considering the mixture effect, and the values of 164.7 GPa and 68.3 GPa are the Young's modulus of the UAl_3 and Aluminum, respectively, which are considered here as the upper and lower bound of the UAl_x-Al fuel meat Young's modulus. As shown in Table 4.2, the predicted maximum radial displacement of MURR HEU plate 24 increases only 0.3 mil when the fuel meat Young's modulus decreases from 164.7 GPa to 68.3 GPa. Therefore, the effect of Young's modulus on the predicted plate displacement is negligible. This is

expected as the impact of elastic properties like Young's modulus will diminish when other irradiation physics are activated. Young's modulus of 84.1 GPa is used in the finalized model.

Table 4.2. Maximum radial displacement predicted using various Young's moduli.

Case	Young's modulus (GPa)	Maximum radial displacement (mil)	Maximum displacement occurs at	Relative difference to Case b
a	164.7	24.0	Irradiation-2	-0.8%
b	**84.1**	24.2	Irradiation-2	**-**
c	68.3	24.3	Irradiation-2	0.3%

The Poisson's ratio of Al is 0.33 [16], and the value of UAl_3 is 0.2 [21]. No data on Poisson's ratio of the UAl_x-Al fuel meat is available in the literature. The value for both UAl_3 and Al will be used in the simulation to evaluate the sensitivity of the results on this material property. Table 4.3 shows that the effect of Poisson's ratio on the predicted plate displacement is negligible, so a Poisson's ratio of 0.33 is used in the finalized model, indicated by bold text in Table 4.3.

Table 4.3. Maximum radial displacement predicted using various Poisson's ratio.

Case	Poisson's ratio	Maximum radial displacement (mil)	Maximum displacement occurs at	Relative difference to Case b
a	0.2	23.9	Irradiation-2	-1.1%
b	**0.33**	24.2	Irradiation-2	**-**

4.1.2 Effects of Coefficient of Thermal Expansion

No data on the CTE of the UAl_x-Al fuel meat was found in the literature. It is expected that the CTE of the UAl_x-Al fuel meat is bounded by the value of UAl_3 and Al (0 wt% U). Therefore, the CTE of both UAl_3 and Al are used in the simulation to evaluate the sensitivity of the results on this material property. At 100 °C, the CTE is around 23.9 × 10^{-6}/K for Aluminum (Case a in Table 4.4) [20] and around 13.3 × 10^{-6}/K for UAl_3 (Case c in Table 4.4) [19]. The best estimate of the fuel meat CTE is calculated as 18.6×10^{-6}/K at 100 °C (Case b in Table 4.4) by extrapolating the data of aluminum-uranium alloys in [19] (data available up to 30 wt% U) to the fuel meat weight fraction of uranium (40.7%) in the MURR HEU fuel system.

Table 4.4 Maximum radial displacement predicted using various CTE.

Case	CTE (10^{-6}/K) at 100 °C	Maximum radial displacement (mil)	Maximum displacement occurs at	Relative difference to Case b
a	23.9	25.5	Irradiation-1	5.2%
b	**18.6**	24.2	Irradiation-2	**-**
c	13.0	22.9	Irradiation-2	-5.5%

As shown in Table 4.4, the maximum radial displacement of the fuel plate can vary up to ±6% compared to the best estimate (Case b). Note that CTE implemented in the T-M model is temperature dependent, only the value at 100 °C is listed for comparison. The best-estimate CTE is used in the finalized model.

Note that for Case a, the maximum displacement occurs at Irradiation-1 and for cases b and c it occurs at Irradiation-2. This difference might be due to the combined effects of thermal expansion and swelling. The plate displacement caused by thermal expansion decreases with irradiation interval due to the decreasing fuel temperature. On the other hand, the plate displacement caused by swelling increases with irradiation interval. For Case a, with higher CTE, the thermal effect is slightly more significant than in other cases, and this may lead to the maximum displacement occurring at Irradiation-1.

4.1.3 Effects of Yield Stress

Although the yield stress data of unirradiated ATR-type UAl_x-Al fuel is available [24], the irradiation effect on the yield stress of the UAl_x-Al fuel is inconclusive, with some data showing increased yield stress due to irradiation, while other data exhibits the opposite effect [24] as discussed in section 3.1.7.

To evaluate the impact of yield stress on the predicted plate displacement, three cases are analyzed. First, elastic material is assumed for the fuel meat, which is equivalent to an infinite yield stress. Second, the yield stress data of unirradiated ATR type UAl_x-Al fuel [24] is used, which is temperature dependent and listed in Table 3.3. The third case uses a lower limit value of 48 MPa based on all data at the relevant temperature range in [24]. The results are shown in Table 4.5. The maximum displacement increases less than 2% when switching from elastic model to elastic-plastic model with lower limit yield stress. In addition, the predicted stress using elastic model are below the lower limit of yield stress (48 MPa) for all irradiation cycles. Therefore, no plasticity model has been implemented in the final model.

Table 4.5. Maximum radial displacement predicted using various yield stress.

Case	Yield stress	Max. radial disp. (mil)	Max. disp. occurs at	Relative difference to Case a
a	**Elastic**	24.2	Irradiation-2	**-**
b	Temperature dependent data (98.5 MPa at 100 °C)	24.3	Irradiation-2	0.2%
c	Lower limit data (48 MPa, constant)	24.6	Irradiation-2	1.6%

4.1.4 Effects of Creep Models

As discussed in Section 3.1.9, no data was found on the irradiation creep of the UAl_x-Al fuel meat in the literature. The aluminum matrix is the continuous phase of the meat and accounts for almost 60% of the volume of the meat. Therefore, it is expected that the creep behavior of the UAl_x-Al fuel meat is similar to that of pure aluminum.

Thermal creep does occur in pure aluminum at room temperature [26], and the thermal creep rate can be calculated using [9]:

$$\dot{\varepsilon} = A\left(\frac{\sigma}{\sigma_0}\right)^n \exp\left(-\frac{Q}{RT}\right) \quad (8)$$

where A is a constant, n is the stress exponent, Q is the activation energy (J/mol) and these three parameters are material-dependent, σ is the stress in MPa, σ_0 is the reference stress of 1 MPa, T is the

temperature in K, and R is gas constant 8.314 J/(mol·K). Using the thermal creep data reported in [29], the A, n, and Q in Equation (5) can be determined to be 9.75×10^{-11} 1/s, 4, and 30 kJ/mol, respectively.

The data on irradiation creep in pure aluminum is sparse and conflicting, with one experiment showing no irradiation creep while the other showed substantial irradiation creep with the enhancement factor (ratio of irradiation creep rate to thermal creep rate) of 10 to 20, as detailed in Farrell [27] and discussed in section 3.1.9.

In this work, the T-M model sensitivity on the creep modeling is evaluated using a wide range of values of the constant A in equation (8). The results of this analysis are shown in Table 4.6. Considering the irradiation creep by increasing the thermal creep rate by a factor of 15 based on an engineering judgment accounting for the enhancement factor mentioned in the earlier paragraph, the maximum displacement only drops 3.3%. Even increasing the thermal creep rate by four orders of magnitude, equivalent to an enhancement factor of ~10000, to represent an extremely significant irradiation creep, the maximum displacement is only 6.5% less than the case that only considers thermal creep. The case without any creep was also analyzed, and an extremely high displacement value was predicted, which is much larger than the outermost coolant channel thickness and is unrealistic since the MURR HEU fuel has demonstrated a safe performance for decades without a single failure. This value is listed here to illustrate the importance of modeling creep in the irradiation thermo-mechanical analyses; otherwise, the model would significantly overestimate the plate deflection.

Table 4.6. Maximum radial displacement predicted using various creep constants.

Case	Creep constant, A (1/s)	Max. radial disp. (mil)	Max. disp. occurs at	Relative difference to Case c
a	9.75×10^{-7}	22.6	Irradiation-1	-6.5%
b	1.46×10^{-9}	23.4	Irradiation-1	-3.3%
c	**9.75×10^{-11}**	24.2	Irradiation-2	**-**
d	No Creep (0)	179.1	Irradiation-4	664.7%

Given that the irradiation creep in aluminum is inconclusive and incorporating the irradiation creep effect by enhancing the thermal creep has a small impact on the plate displacement, only thermal creep is considered in the finalized model.

4.1.5 Effects of Swelling Models

Two swelling correlations are provided in Section 3.1.8. For the maximum fission density used in this work, one correlation [24] predicts 3.9% volumetric swelling while the other predicts 1.4% [25] volumetric swelling. Both correlations are used in the sensitivity analysis, and the results is shown in Table 4.7. Although the correlation from [24] indicates more than two-fold higher fuel core swelling, the T-M models using these two correlations show only 1.3 mil difference in the maximum radial displacements. The swelling correlation by Beeston et al. [24] is used in the finalized model, though the Beeston and Miller could also be used since it represents a later data evaluation..

Table 4.7. Maximum radial displacement predicted using various swelling correlations.

Case	Swelling correlation	Max. radial disp. (mil)	Max. disp. occurs at	Relative difference to Case a
a	**Beeston et al. [24]**	24.2	Irradiation-2	-
b	Miller and Beeston [25]	22.9	Irradiation-1	-5.4%

4.2 Model Sensitivity on Coolant Conditions

The FE model employed coolant temperature and HTC distribution from the prototypic MURR HEU operation as boundary conditions at the plate surfaces. The existing PLTEMP/ANL model for the TH analysis includes HCFs to account for the uncertainties from manufacturing, calculations, and channel gap reductions from the burnup-related effects. In addition, the model is constructed to evaluate one stripe out of nine at a time.

In this section, the sensitivity of the FE model on the predicted coolant conditions was assessed by considering the four different combinations of TH model inputs: with or without HCFs, and coolant conditions for the hottest stripe (either stripe 1 or 9) or the coldest stripe (stripe 5). The set of HCFs used for this sensitivity analysis is outlined in Table 2.4.

Coolant temperature distributions evaluated in the FE model are shown in Figure 4.1. The inlet temperature is about 48.89 °C (120 °F). The temperature rise for channel 24 is higher than that of channel 25, since channel 24 is heated by both plate 23 and 24, while channel 25 is heated only by plate 24. With HCFs, the coolant temperature rise is greater, up to 10.8%. The difference in coolant temperature between coldest stripe and hottest stripe is very small.

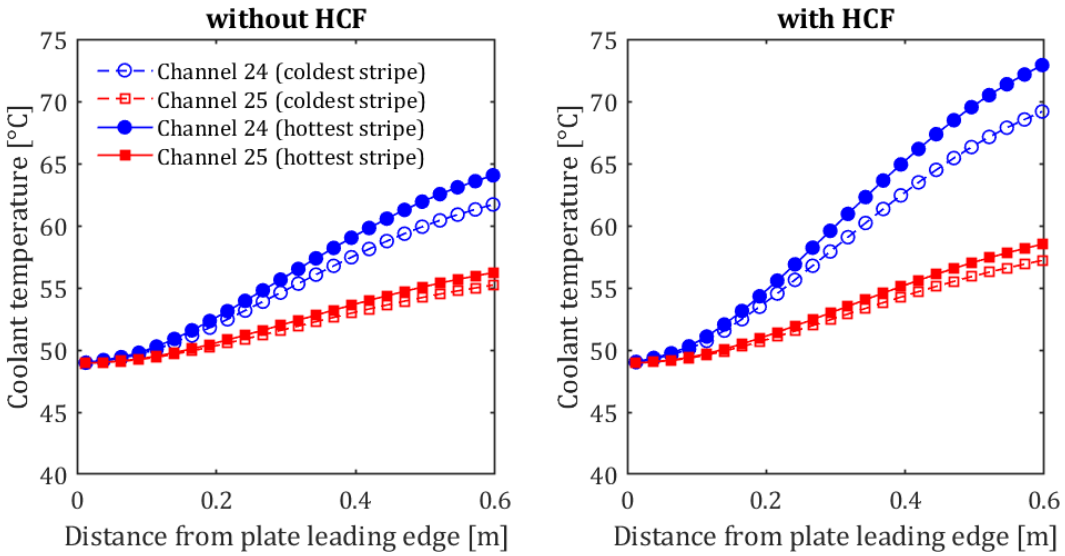

Figure 4.1. Coolant temperature distributions from the TH analysis.

The HTC evaluated in the FE model are shown in Figure 4.2. The HTC are the same for different stripes. The HTC with HCFs is less that that without them.

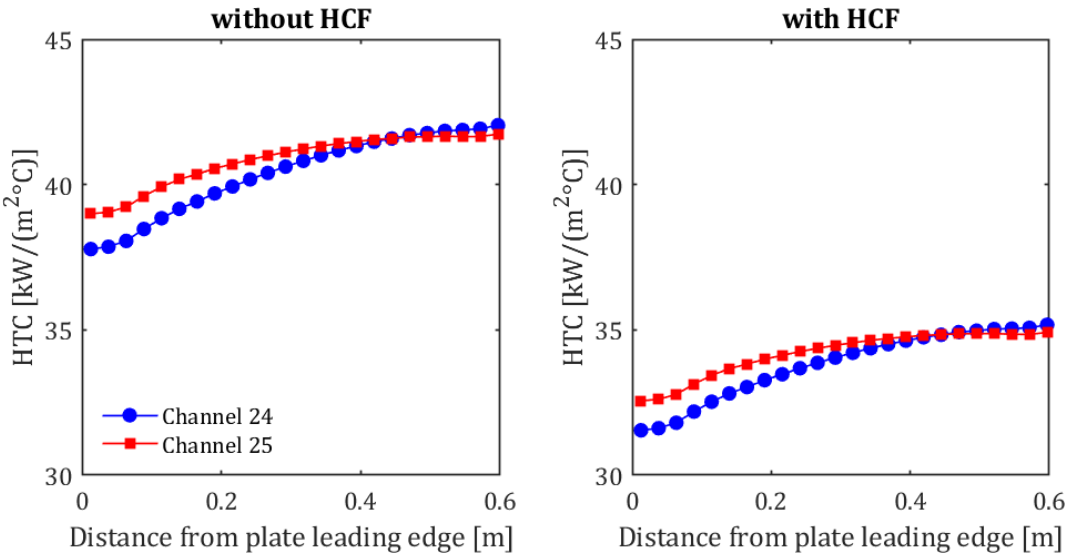

Figure 4.2. Heat Transfer Coefficient distributions from the TH analysis.

The results of the model sensitivity on coolant condition are shown in Table 4.8. Either using coolant temperature from the hottest or the coldest stripe has negligible impact on the results. The best estimate (without HCFs) coolant conditions from the hottest stripe is used in the finalized model. Including the HCFs increases the maximum displacement by about 11%.

Table 4.8. Maximum radial displacement predicted using various cooling conditions.

Case	Evaluated stripe	With or without HCFs	Max. radial disp. (mil)	Max. disp. occurs at	Relative difference to Case a
a	**hottest stripe**	**without HCFs**	**24.1**	**Irradiation-2**	**-**
b	coldest stripe	without HCFs	23.8	Irradiation-2	-1.2%
c	hottest stripe	with HCFs	26.7	Irradiation-2	10.8%
d	coldest stripe	with HCFs	26.2	Irradiation-2	8.7%

4.3 Summary of Model Sensitivity

The predicted maximum displacement is almost insensitive to the elastic modulus and Poisson's ratio of the HEU fuel meat, with a variance of 1% within the bounding range. The maximum radial displacement of the fuel plate can vary up to ±6% by changing the best-estimate CTE to the upper/lower bounding. No plasticity model has been implemented in the finalized model because the predicted stress using elastic model are below the lower limit of yield stress (48 MPa) for all irradiation cycles.

Thermal creep of aluminum was considered in the model, and the effect of irradiation creep was evaluated by increasing the thermal creep rate by factors of 15 and 10000. The maximum displacement drops 3.3% and 6.5%, respectively, due to the increased creep rate. Two swelling correlations were evaluated in this work, which predict 3.9% and 1.4% swelling volumetric change at the maximum fission density. The difference in maximum displacement from the T-M models using these two correlations is around 5%.

Coolant conditions i.e., coolant temperature and HTC distribution, taken from the hottest and coldest stripe from the TH analysis did not show a considerable impact on the calculated maximum radial displacements for plate 24 (0.5 mil). Including the HCFs increases the maximum displacement by about 11%.

The material properties and behavior models selected for the baseline model usually predict slightly higher plate deflection than the models used for the sensitivity analysis. Therefore, a 15% engineering factor appears appropriate for the channel gap reduction for the types of analysis that require conservatism to accommodate the impact of variations in coolant conditions and uncertainties in material properties and behavior models.

5 Results and Discussion

This section presents the FE simulation results for the irradiation T-M behavior of the MURR HEU fuel plate 24 under the prototypic irradiation conditions. The model uses the coolant conditions at the hottest stripe from the TH analysis without HCFs, thus representing the best estimate case. From the calculated radial displacements of fuel plate 24 from the FE simulations, the coolant channel 25 gap thickness changes are reported on the grid used for the TH safety basis modeling.

5.1 Fuel Plate 24 Displacement

Figure 5.1 shows the radial displacement of plate 24 at the end of each irradiation interval, as well as the beginning-of-life (BOL) step. The BOL step in the T-M model only considers thermal effects i.e., thermal expansion, while the irradiation effects like swelling and creep are not active yet. A steady-state shutdown step is also analyzed, which set the fuel plate to a constant temperature, and the results are discussed in Appendix B.

Under the applied mechanical constraints and loads due to the irradiation and thermal conditions, the curved fuel plate deflects towards the convex side of the plate in the radial direction (normal to the plate surface). In the lateral direction (y), the radial displacement profile is almost symmetric with respect to the lateral centerline because the neutronics data are almost symmetric. Over the life of the element, the peak radial deflection is calculated as 24.1 mil at the end of Irradiation-2 on the lateral centerline.

Table 5.1 lists the maximum radial displacements for all irradiation intervals, including the BOL step. The BOL maximum radial displacement is about 86% of the peak (Irradiation-2) maximum radial displacement. Given that only the thermal loads are applied to the fuel plate at the startup step to calculate BOL results, the thermal loads have a significant impact on the plate radial displacement under the assumed mechanical constraints for the plate-level model. This observation is consistent with the counterpart LEU plate-level modeling results [8].

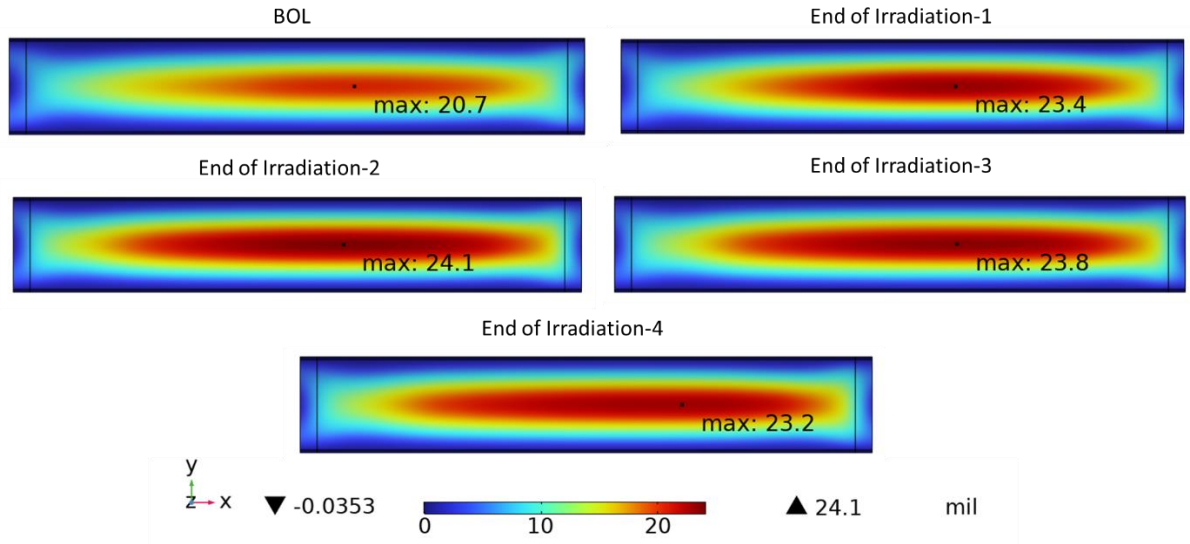

Figure 5.1. Plate 24 radial displacements at the end of irradiation intervals.

Table 5.1. Calculated maximum radial displacement for plate 24.

Step	Max. radial disp. (mil)
BOL	20.7
Irradiation-1 (48 hr)	23.4
Irradiation-2 (1409 hr)	24.1
Irradiation-3 (1560 hr)	23.8
Irradiation-4 (2873 hr, EOL)	23.2

5.2 Coolant Channel 25 Gap Reduction for the TH Analysis

The fuel plates deflect and swell during the irradiation, which results in changes in the thickness of the coolant gaps. The coolant gap thickness reduction is estimated following a procedure that maps FE results to the respectively coarser grid for the MURR TH analysis via spatial averaging. This procedure provides more relevant input for TH analyses. Consequently, the results in this section are presented on the grid relevant to the nodal resolution used in the MURR TH analysis [2]. The nine stripes in the azimuthal direction are also shown in Figure 2.4.

Coolant channel 25 gap is situated between the outermost fuel plate 24 and the outer pressure vessel wall.

Figure 5.2 shows the coolant channel 25 gap thickness change on the TH grid at the end of each irradiation interval. It should be noted that the negative values in Figure 5.2 indicate a reduction in coolant gap thickness. The model shows the nodal maximum coolant channel thickness reduction magnitude of 23.4 mil on stripe 5.

In addition to the nodal maximum, the stripe-averaged channel thickness reduction is of interest for the TH analysis. The stripe-averaged results are listed in Table 5.2. The maximum stripe-average channel 25 gap reduction occurs at the end of Irradiation-2 for stripe 5, with the value of 20.1 mil.

End of Irradiation-1 (48 h)

-0.7	-2.0	-3.4	-6.2	-7.7	-6.2	-3.4	-2.0	-0.7
-0.4	-1.3	-2.7	-7.0	-10.7	-7.0	-2.7	-1.3	-0.4
-0.3	-1.2	-2.7	-7.9	-12.6	-7.9	-2.7	-1.2	-0.3
-0.4	-1.5	-3.1	-9.0	-14.2	-9.0	-3.1	-1.5	-0.4
-0.5	-1.8	-3.7	-10.2	-15.8	-10.2	-3.7	-1.8	-0.5
-0.6	-2.0	-4.2	-11.2	-17.2	-11.2	-4.2	-2.0	-0.6
-0.6	-2.2	-4.5	-12.1	-18.4	-12.0	-4.5	-2.2	-0.6
-0.7	-2.3	-4.8	-12.7	-19.3	-12.7	-4.8	-2.3	-0.6
-0.7	-2.4	-5.0	-13.3	-20.1	-13.2	-5.0	-2.4	-0.7
-0.7	-2.5	-5.2	-13.7	-20.8	-13.7	-5.2	-2.5	-0.7
-0.7	-2.6	-5.4	-14.2	-21.5	-14.2	-5.4	-2.6	-0.7
-0.7	-2.7	-5.5	-14.6	-22.1	-14.6	-5.5	-2.7	-0.7
-0.8	-2.7	-5.6	-14.8	-22.5	-14.8	-5.6	-2.7	-0.8
-0.8	-2.7	-5.6	-14.9	-22.6	-14.9	-5.6	-2.7	-0.8
-0.8	-2.7	-5.7	-14.9	-22.7	-14.9	-5.6	-2.7	-0.8
-0.8	-2.7	-5.6	-14.9	-22.6	-14.8	-5.6	-2.7	-0.8
-0.8	-2.7	-5.6	-14.7	-22.4	-14.7	-5.5	-2.7	-0.8
-0.7	-2.6	-5.4	-14.5	-22.1	-14.4	-5.4	-2.6	-0.7
-0.7	-2.5	-5.2	-14.0	-21.5	-14.0	-5.2	-2.5	-0.7
-0.6	-2.3	-4.8	-13.4	-20.7	-13.4	-4.8	-2.3	-0.6
-0.6	-2.1	-4.4	-12.5	-19.7	-12.5	-4.4	-2.1	-0.6
-0.6	-2.0	-4.2	-11.6	-18.1	-11.6	-4.2	-2.0	-0.6
-0.8	-2.4	-4.6	-10.9	-15.9	-10.9	-4.6	-2.4	-0.8
-1.2	-3.4	-5.5	-9.6	-11.8	-9.6	-5.5	-3.4	-1.2

End of Irradiation-2 (1409 h)

-0.7	-2.2	-3.8	-7.5	-9.7	-7.5	-3.8	-2.2	-0.7
-0.5	-1.6	-3.3	-8.6	-13.0	-8.6	-3.3	-1.6	-0.5
-0.4	-1.6	-3.4	-9.5	-14.8	-9.5	-3.4	-1.6	-0.4
-0.5	-1.9	-3.9	-10.7	-16.6	-10.7	-3.9	-1.9	-0.6
-0.7	-2.2	-4.5	-12.0	-18.3	-12.0	-4.5	-2.2	-0.7
-0.8	-2.5	-5.0	-13.0	-19.7	-13.0	-5.0	-2.5	-0.8
-0.8	-2.7	-5.3	-13.7	-20.7	-13.7	-5.3	-2.7	-0.8
-0.9	-2.8	-5.6	-14.2	-21.4	-14.2	-5.6	-2.8	-0.9
-0.9	-2.9	-5.8	-14.7	-22.0	-14.6	-5.8	-2.9	-0.9
-1.0	-3.0	-5.9	-15.0	-22.5	-15.0	-5.9	-3.0	-1.0
-1.0	-3.1	-6.0	-15.2	-22.9	-15.2	-6.0	-3.1	-1.0
-1.0	-3.1	-6.1	-15.4	-23.1	-15.5	-6.1	-3.1	-1.0
-1.0	-3.1	-6.2	-15.5	-23.3	-15.5	-6.2	-3.1	-1.0
-1.0	-3.1	-6.2	-15.6	-23.4	-15.6	-6.2	-3.1	-1.0
-1.0	-3.1	-6.2	-15.6	-23.4	-15.6	-6.2	-3.1	-1.0
-1.0	-3.1	-6.1	-15.5	-23.3	-15.5	-6.1	-3.1	-1.0
-1.0	-3.1	-6.1	-15.4	-23.2	-15.4	-6.1	-3.1	-1.0
-1.0	-3.0	-5.9	-15.2	-23.0	-15.2	-5.9	-3.0	-1.0
-0.9	-2.9	-5.7	-14.9	-22.6	-14.9	-5.7	-2.9	-0.9
-0.8	-2.7	-5.4	-14.4	-22.0	-14.3	-5.4	-2.7	-0.8
-0.8	-2.5	-5.1	-13.7	-21.2	-13.7	-5.1	-2.5	-0.8
-0.7	-2.4	-4.9	-12.9	-19.8	-12.9	-4.9	-2.4	-0.7
-1.0	-2.9	-5.3	-12.4	-17.9	-12.4	-5.3	-2.9	-1.0
-1.4	-3.7	-6.1	-10.9	-13.7	-10.9	-6.0	-3.7	-1.4

End of Irradiation-3 (1560 h)

-0.7	-2.1	-3.7	-7.1	-9.2	-7.1	-3.7	-2.1	-0.7
-0.5	-1.6	-3.2	-8.1	-12.2	-8.1	-3.2	-1.6	-0.5
-0.4	-1.6	-3.3	-9.0	-14.0	-8.9	-3.2	-1.5	-0.4
-0.5	-1.8	-3.8	-10.3	-15.9	-10.3	-3.8	-1.8	-0.6
-0.7	-2.2	-4.4	-11.6	-17.8	-11.7	-4.4	-2.2	-0.7
-0.8	-2.5	-4.9	-12.7	-19.3	-12.7	-4.9	-2.5	-0.8
-0.8	-2.7	-5.2	-13.4	-20.2	-13.4	-5.3	-2.7	-0.8
-0.9	-2.8	-5.5	-13.9	-21.0	-14.0	-5.5	-2.8	-0.9
-0.9	-2.9	-5.7	-14.4	-21.6	-14.4	-5.7	-2.9	-0.9
-1.0	-3.0	-5.8	-14.7	-22.0	-14.7	-5.9	-3.0	-1.0
-1.0	-3.0	-6.0	-15.0	-22.4	-15.0	-6.0	-3.1	-1.0
-1.0	-3.1	-6.0	-15.2	-22.7	-15.2	-6.0	-3.1	-1.0
-1.0	-3.1	-6.1	-15.3	-22.9	-15.3	-6.1	-3.1	-1.0
-1.0	-3.1	-6.1	-15.4	-23.0	-15.4	-6.1	-3.1	-1.0
-1.0	-3.1	-6.1	-15.4	-23.1	-15.4	-6.1	-3.1	-1.0
-1.0	-3.1	-6.1	-15.4	-23.0	-15.3	-6.1	-3.1	-1.0
-1.0	-3.1	-6.0	-15.3	-23.0	-15.3	-6.0	-3.1	-1.0
-1.0	-3.0	-5.9	-15.1	-22.8	-15.1	-5.9	-3.0	-1.0
-0.9	-2.9	-5.7	-14.8	-22.4	-14.8	-5.7	-2.9	-0.9
-0.8	-2.7	-5.4	-14.3	-21.9	-14.2	-5.4	-2.7	-0.8
-0.8	-2.5	-5.0	-13.6	-21.0	-13.6	-5.0	-2.5	-0.8
-0.8	-2.4	-4.9	-12.8	-19.6	-12.8	-4.8	-2.4	-0.8
-1.0	-2.8	-5.3	-12.2	-17.7	-12.2	-5.3	-2.8	-1.0
-1.4	-3.7	-6.0	-10.7	-13.6	-10.7	-6.0	-3.7	-1.4

End of Irradiation-4 (2873 h)

-0.8	-2.2	-3.8	-7.3	-9.5	-7.4	-3.8	-2.2	-0.8
-0.5	-1.6	-3.2	-8.3	-12.5	-8.3	-3.3	-1.6	-0.5
-0.5	-1.6	-3.3	-9.2	-14.3	-9.2	-3.3	-1.6	-0.5
-0.6	-1.9	-3.9	-10.5	-16.2	-10.5	-3.9	-1.9	-0.6
-0.8	-2.3	-4.5	-11.8	-17.9	-11.7	-4.5	-2.3	-0.8
-0.9	-2.6	-5.0	-12.8	-19.2	-12.7	-5.0	-2.6	-0.9
-1.0	-2.8	-5.4	-13.4	-20.0	-13.3	-5.3	-2.8	-1.0
-1.1	-3.0	-5.6	-13.8	-20.7	-13.8	-5.6	-3.0	-1.0
-1.1	-3.0	-5.8	-14.2	-21.1	-14.2	-5.8	-3.0	-1.1
-1.1	-3.1	-5.9	-14.5	-21.5	-14.5	-5.9	-3.1	-1.1
-1.1	-3.2	-6.0	-14.7	-21.8	-14.7	-6.0	-3.2	-1.1
-1.2	-3.2	-6.1	-14.9	-22.1	-14.9	-6.1	-3.2	-1.2
-1.2	-3.3	-6.1	-15.0	-22.2	-15.0	-6.1	-3.2	-1.2
-1.2	-3.3	-6.2	-15.1	-22.4	-15.1	-6.2	-3.3	-1.2
-1.2	-3.3	-6.2	-15.1	-22.5	-15.1	-6.2	-3.3	-1.2
-1.2	-3.2	-6.2	-15.1	-22.5	-15.1	-6.2	-3.2	-1.2
-1.1	-3.2	-6.1	-15.1	-22.5	-15.1	-6.1	-3.2	-1.1
-1.1	-3.1	-6.0	-14.9	-22.4	-14.9	-6.0	-3.1	-1.1
-1.1	-3.0	-5.8	-14.7	-22.2	-14.7	-5.8	-3.0	-1.1
-1.0	-2.8	-5.5	-14.2	-21.7	-14.2	-5.5	-2.8	-1.0
-0.9	-2.6	-5.1	-13.6	-20.9	-13.6	-5.1	-2.6	-0.9
-0.9	-2.5	-4.9	-12.9	-19.6	-12.9	-4.9	-2.5	-0.9
-1.1	-2.9	-5.4	-12.3	-17.7	-12.3	-5.4	-2.9	-1.1
-1.5	-3.8	-6.1	-10.8	-13.6	-10.8	-6.1	-3.8	-1.5

Figure 5.2. Coolant channel 25 thickness reduction on TH node at the end of each irradiation interval.

Table 5.2. Coolant channel 25 thickness reduction on TH stripes at the end of irradiation intervals.

	Stripe-averaged value (mil)				
	BOL	Irradiation-1 (48 hr)	Irradiation-2 (1409 hr)	Irradiation-3 (1560 hr)	Irradiation-4 (2873 hr)
Stripe 1/9	-0.6	-0.7	-0.9	-0.9	-1.0
Stripe 2/8	-2.1	-2.3	-2.7	-2.7	-2.8
Stripe 3/7	-4.2	-4.7	-5.3	-5.3	-5.3
Stripe 4/6	-10.9	-12.2	-13.4	-13.2	-13.1
Stripe 5	-16.5	-18.5	**-20.1**	-19.7	-19.5

5.3 Comparison to LEU Results

One motivation of this work is to compare the behavior of the MURR HEU from this work and LEU fuel plates [8] under the prototypic thermal and irradiation conditions. The modeling approach for the HEU analysis follows that of LEU analysis but with all geometry information, neutronics and TH data, material properties and behavioral models (swelling and creep) relevant for the MURR HEU core.

Table 5.3 compares the maximum stripe-averaged outermost coolant channel reduction between the HEU and LEU fuel elements. The magnitude of the outermost coolant channel reduction i.e., channel 25 for HEU and 24 for LEU, is similar between HEU and LEU. For HEU, the maximum stripe-averaged channel reduction of 20.1 mil occurs at the end of Irradiation-2, while for LEU the maximum stripe-averaged channel reduction of 20.6 mil occurs at the end of Irradiation-4. Despite the different dimensions of HEU plate 24 and MURR plate 23, non-linearity of the T-M model (e.g., the temperature dependence of material properties) as well as the differences between the U-10Mo monolithic LEU fuel and the UAl_x-Al dispersion fuel, including material properties, material degradation under irradiation, and behavior models, the maximum deflections of MURR HEU plate 24 and MURR LEU plate 23, and consequently the reduction in the outermost end channels, are of a similar magnitude.

Table 5.3. Comparison of maximum outer coolant channel reduction on TH node between HEU and LEU.

	Max. stripe-averaged outermost coolant channel reduction (mil)				
	Start-up	Irradiation-1 (48 hr for both HEU and LEU)	Irradiation-2 (1409 hr for HEU, 1258 h for LEU)	Irradiation-3 (1560 hr for both HEU and LEU)	Irradiation-4 (2873 hr for both HEU and LEU)
HEU	-16.5	-18.5	-20.1	-19.7	-19.5
LEU [8]	-16.8	-19.1	-20.1	-20.4	-20.6
Relative difference to LEU	-1.5%	-3.4%	-0.2%	-3.5%	-5.5%

In addition to plate-level analysis, element-level T-M analysis is also performed for MURR LEU element [30], in which 23 fuel plates, side plates, and combs are modeled. The maximum stripe-average channel reduction occurs at EOL on channel 24 middle stripe, which is 13.5 mil. This is 34%

less than that of plate-level analysis. When the effect of oxide layer thermal resistance is considered in the MURR LEU element-level model, the maximum stripe-averaged channel reduction increases to 15.9 mil [30]. Given that the plate-level models for HEU and LEU predicts similar magnitude of coolant channel reductions, it is not expected that the element-level analysis of HEU element would predict a substantially different value compared to the LEU element-level results.

Furthermore, MURR TH analyses have been completed in a separate work to evaluate the impact of the predicted changes in channel thickness. The results show that MURR maintains sufficient margins in HEU and LEU cores [31].

6 Summary

In this work, the T-M analysis of MURR HEU fuel plate 24 was performed to compare it with that of the MURR LEU plate. The modeling approach for the HEU analysis follows that of the LEU analysis [8], but with all geometry information, neutronics and TH data, material properties and behavioral models relevant for the HEU conditions. Mapping the FE model results to the same grid for the TH safety basis modeling, the thickness change for the coolant channel gap 25 was calculated.

FE model sensitivity to the fuel meat material properties and behavior models (swelling and creep) were analyzed to determine the baseline model. The sensitivity of the maximum displacement was found to be negligible to the elastic modulus and Poisson's ratio of the HEU fuel meat, with a variance of 1% within the bounding range. The maximum radial displacement of the fuel plate could vary up to ±6% by changing the best estimate CTE to the upper and lower bounding. No plasticity model was implemented in the final model because the computed stresses using elastic model were below the lower limit of yield stress (48 MPa) for all irradiation cycles. Thermal creep of aluminum was considered in the model, and the effect of the irradiation creep was evaluated by increasing the thermal creep rate by factors of 15 and 10000. The maximum displacement drops by 3.3% and 6.5%, respectively, due to the increased creep rate. Two swelling correlations were evaluated in this work, which predict 3.9% and 1.4% swelling volumetric change at the maximum fission density. The difference in maximum displacement from the T-M models using these two correlations is around 5%. FE model sensitivity to the coolant conditions is also investigated. Coolant conditions (coolant temperature and HTC distributions) taken from the hottest or coldest stripe (from the TH analysis) did not show a considerable impact on the calculated maximum radial displacements for plate 24 (0.5 mil). A 15% engineering factor appears appropriate for the channel gap reduction for the types of analysis that require conservatism to accommodate the impact of variations in coolant conditions and uncertainties in material properties and behavior models.

The findings related to the reduction in channel 25 of MURR HEU element due to the irradiation thermo-mechanical analysis behavior of plate 24 are summarized below:

1. The maximum stripe-averaged outermost channel (channel 25) reduction for the MURR HEU fuel is 20.1 mil, which occurs at the middle stripe (stripe 5). This value is comparable to that of MURR LEU fuel predicted by the plate-level model (20.6 mil). The stripe-averaged channel 25 reduction for the hottest stripe (stripe 1/9) of 1.0 mil is smaller than the assumed value of 5 mil used in the previous safety analysis report. Edge stripes were analyzed previously due to the edge peaking of power. However, although the power is also lower in the center stripe, TH analysis should also be performed on other stripes including the center stripe.
2. At the BOL with only thermal loads, a stripe-averaged displacement up to 16.5 mil is predicted, and this increases to only 20.1 mil throughout the life of the element. Consistent with LEU model observations, this indicates that thermal expansion plays a significant role.

In addition to plate-level analysis, element-level T-M analysis is performed for MURR LEU element , which predicts 34% less maximum stripe-average channel reduction. Given that the plate-level models for HEU and LEU predict similar magnitude of coolant channel reductions, if element-level modeling were performed for the HEU element, as it has been for LEU, then significantly smaller reductions in the channels would be expected than determined in this work. Furthermore, MURR TH analyses have been completed in a separate work to evaluate the impact of the predicted changes in channel thickness. The results show that MURR maintains sufficient margins in HEU and LEU cores.

Acknowledgement

Caleb Braun and Kiratadas Kutikkad of University of Missouri Research Reactor (MURR) are gratefully acknowledged for contributions to reactor conversion, including information about the works referenced. The authors would like to thank Drs. Marta Sitek, Medhat Sharabi, and Laura Jamison of Argonne National Laboratory (Argonne) for review of this work, as well as Drs. Gerard Hofman, Bei Ye, Zhi-Gang Mei, and Wilson Cowherd of Argonne for the valuable discussions.

This work was sponsored by the U.S. Department of Energy, Office of Material Management and Minimization in the U.S. National Nuclear Security Administration Office of Defense Nuclear Nonproliferation under Contract DE-AC02-06CH11357.

References

1. E. Wilson, et al., "US high performance research reactor conversion program: An overview on element design," European Research Reactor Conference, Rotterdam, Netherlands, 2017.
2. J. Stillman, et al.; *Transition Core Planning and Safety Analyses in Support of LEU Fuel Conversion of the University of Missouri Research Reactor (MURR)*. ANL/RTR/TM-19/18, Argonne National Laboratory, Lemont, USA, Sep. 2020.
3. J. A. Stillman, et al.; *Low-Enriched Uranium Conversion Preliminary Safety Analysis Report for the University of Missouri Research Reactor*. University of Missouri Research Reactor, Columbia, USA, Aug. 2017.
4. J. Stillman, et al.; *Safety Analysis of the Mo-99 Production Upgrade to the University of Missouri Research Reactor (MURR) with Highly-Enriched and Low-Enriched Uranium Fuel*. ANL/RTR/TM-18/16, Argonne National Laboratory, Lemont, USA, Oct. 2019.
5. *Guidelines for Preparing and Reviewing Applications for the Licensing of Non-Power Reactors, Format and Content, NUREG-1537, Part 1*, United States Nuclear Regulatory Commission, February 1996
6. *Guidelines for Preparing and Reviewing Applications for the Licensing of Non-Power Reactors, Standard Review Planned Acceptance Criteria, NUREG-1537, Part 2*, United States Nuclear Regulatory Commission, February 1996
7. W. Mohamed, et al., *Fuel Swelling and Creep Analysis for a MURR LEU U-10Mo Monolithic Plate, ANL/RTR/TM-18/19*, Argonne National Laboratory, Lemont, USA, Mar. 2019
8. Firat Cetinbas, et al.; *Thermo-Mechanical Analysis of Irradiated MURR LEU Fuel Plates*. ANL/RTR/TM-23/11, Argonne National Laboratory, Lemont, IL, Mar. 2023.
9. *COMSOL Multiphysics® v. 6.1 www.comsol.com. COMSOL AB, Stockholm, Sweden*,
10. *Missouri University Research Reactor (MURR) Safety Analysis Report*, Missouri University Research Reactor, Columbia, USA, 2006
11. E. E. Feldman, et al.; *Technical Basis in Support of the Conversion of the University of Missouri Research Reactor (MURR) Core from Highly-Enriched to Low-Enriched Uranium - Steady-State Thermal-Hydraulic Analysis*. ANL/RERTR/TM-12-37 Rev. 1, Argonne National Laboratory, Lemont, USA, Jan. 2013.
12. X-5 Monte Carlo Team; *MCNP- A General Monte Carlo N-Particle Transport Code, Version 5*. Los Alamos National Laboratory, Los Alamos, USA, 2003.
13. N. J. Peters; *Spatial Distribution of the Effective Fission Energy Deposition within the MURR Core: HEU vs. LEU Fuel Comparison*. TDR-0140, University of Missouri Research Reactor, Columbia, USA, 2015.
14. M. Kalimullah, A. P. Olson and E. E. Feldman; *A User's Guide to the PLTEMP/ANL Code (V.4.3)*. ANL/RTR/TM-18/17-Rev.02, Argonne National Laboratory, Lemont, USA, 2021.
15. J. E. Matos and J. L. Snelgrove, *Research reactor core conversion guidebook-Vol 4: Fuels (Appendices IK)*, IAEA, 1992
16. A. I. H. Committee, *Properties of Pure Metals, Properties and Selection: Nonferrous Alloys and Special-Purpose Materials*, ed. R. T. Webster, ASM International, 1990.
17. J. A. Stillman, et al.; *Accident Analyses for Conversion of the University of Missouri Research Reactor (MURR) from Highly-Enriched to Low-Enriched Uranium*. ANL/GTRI/TM-14/5, Revision 1, Argonne National Laboratory, Lemont, USA, Feb. 2017.
18. L. Jamison, et al.; *Review of the Technical Basis for Properties and Fuel Performance Data Used in HEU to LEU Conversion Analysis for U-10Mo Monolithic Alloy Fuel*. ANL/RTR/TM-17/19 Rev.1, Argonne National Laboratory, Lemont, IL, 2020.
19. H. B. Peacock and R. L. Frontroth, *Properties of aluminum-uranium alloys*, Savannah River Site (SRS), Aiken, SC, USA, 1989

20. *Metals Handbook, 1948 Edition*, American Society for Metals, 1948.
21. Z.-G. Mei and A. M. Yacout, "First-principles study of structural, elastic, electronic, vibrational and thermodynamic properties of uranium aluminides," *Computational Materials Science*, 158, p. 26-31 (2019).
22. J. Rest, et al.; *U-Mo Fuels Handbook*. ANL-09/31, Argonne National Laboratory, Lemont, IL, 2009.
23. B. Rabin, et al., *Preliminary Report on U-Mo Monolithic Fuel for Research Reactors*, Idaho National laboratory, Idaho Falls, Idaho, March 2020
24. J. M. Beeston, et al., "Development and irradiation performance of Uranium Aluminide fuels in test reactors," *Nuclear Technology*, 49(1), p. 136-149 (1980).
25. L. Miller and J. Beeston; *Extended life aluminide fuel. Final report*. EGG-2441, EG and G Idaho, Inc., Idaho Falls (USA), 1986.
26. K. Farrell; *Assessment of Aluminum Structural Materials for Service Within the ANS Reflector Vessel*. ORNL/TM-13049, Oak Ridge National Laboratory, Oak Ridge, TN, USA, 1995.
27. K. Farrell; *Materials Selection for the HFIR Cold Neutron Source*. ORNL/TM-99-208, Oak Ridge National Laboratory, Oak Ridge, TN, 2001.
28. C. Bojanowski, et al.; *Impact of MURR LEU Conversion on Beryllium Reflector Lifetime*. ANL/RTR/TM-20/1, Argonne National Laboratory, Lemont, IL, 2020.
29. T. Matsunaga and E. Sato, "Creep mechanism in several grades of aluminum at low temperatures," *Journal of Japan Institute of Light Metals*, 64(2), p. 42-48 (2014).
30. F. Cetinbas, et al.; *Preliminary Thermo-Mechanical Analysis of Irradiated MURR LEU Fuel Element* ANL/RTR/TM-23/19, Argonne National Laboratory, Lemont, IL, 2024.
31. D. S. Yoon, et al.; *Impacts of Irradiation Structural Behavior on Thermal Hydraulics Safety Analysis to Support MURR LEU Conversion*. ANL/RTR/TM-23/27, Argonne National Laboratory, Lemont, IL, 2024.

Appendix A: Mesh Sensitivity

The mesh employed for FE analysis was constructed by sweeping the convex surface mesh through the thickness of each domain in the plate. Mesh sensitivity analysis was performed based on maximum radial displacement for the finalized model.

Firstly, the in-plane mesh sensitivity was analyzed by fixing the through the thickness finite element number as follows: two layers of elements in half thickness of fuel meat and two layers of mesh in AA6061 cladding.

Table A.1 shows that refining the in-plane mesh has a negligible impact on the maximum radial displacement. The in-plane mesh with the element number of 48576 is selected, which is highlighted in bold font in the table.

Table A.1. Model sensitivity to the in-plane mesh

Number of elements	Max. radial disp. (mil)
14136	23.8
48576	**24.2**
76024	24.1
115232	24.2

Next, keeping the in-plane mesh profile obtained with 48576 elements, sensitivity to the number of mesh layers in the fuel meat and AA6061 was analyzed. Table A.2 shows the model sensitivity to the through-the-thickness mesh, and the number in the first column is the number of layers for mesh in half thickness of fuel meat as well as the number of layers of mesh in AA6061 cladding. The difference between through-thickness mesh configuration mesh 1-1, 2-2, and 3-3 is negligible. The through-the-thickness with two layers for both half thickness of fuel meat and AA6061 cladding is selected, which is given in bold font in the table.

Table A.2. Model sensitivity to the through-thickness mesh

Through-thickness mesh configuration	Max. radial disp. (mil)
1-1	24.2
2-2	**24.2**
3-3	24.3

Appendix B: Plate displacement after shutdown

After the end of irradiation-4 (2873 hr), a steady-state shutdown step is analyzed in the T-M model. This step excludes the power generation and brings the fuel plate to a constant temperature of 52 °C, which simulates the permanent deformation of the fuel after being discharged from the core. The fuel temperature of 52 °C is higher than the pool outlet temperature of 40.6 °C [10] and should be a reasonable approximation of the plate temperature considering the heat decay. Similar approximation had been used to estimate fuel temperature after irradiation for other fuel, as discussed in 3.7.2 of [18].

Note that this shutdown step is a steady-state simulation, so any rate-dependence of the material properties are not considered. The Plate 24 radial displacements after the showdown step is shown in Figure B.1. The maximum value is 17.6 mil, which is 27% less than the peak radial deflection of 24.1 mil at the end of Irradiation-2. In addition, the displacement is averaged over the TH stripes, as listed in Table B.1, in case comparing the stripe-averaged values becomes relevant later.

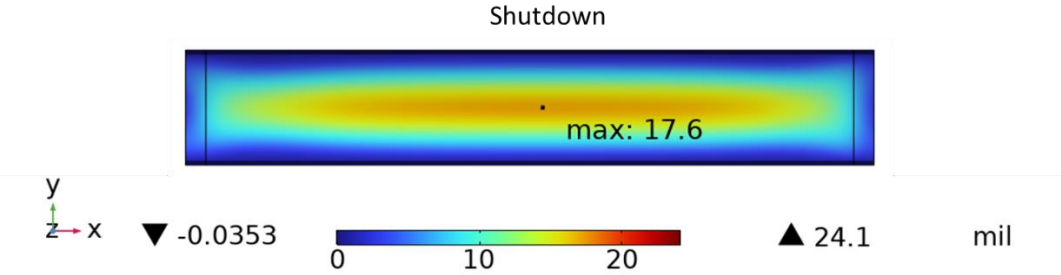

Figure B.1. Plate 24 radial displacements after the showdown step.

Table B.1. Plate 24 radial displacements on TH stripes after the showdown step.

	Stripe-averaged value (mil)
Stripe 1/9	0.9
Stripe 2/8	2.4
Stripe 3/7	4.4
Stripe 4/6	10.5
Stripe 5	15.4

Nuclear Science & Engineering Division
Argonne National Laboratory
9700 South Cass Avenue, Bldg. 208
Argonne, IL 60439

www.anl.gov

Argonne National Laboratory is a U.S. Department of Energy laboratory managed by UChicago Argonne, LLC